# Ediacaran coupling of climate and biosphere dynamics

**Thomas W. Wong Hearing[1], Benjamin Tindal[2], Thomas Vandyk[1], Lin Na[1,3], Alexandre Pohl[4], Alexander G. Liu[5], Thomas H. P. Harvey[1], Mark Williams[1]**

[1]*Centre for Palaeobiology and Biosphere Evolution, School of Geography, Geology and the Environment, University of Leicester, Leicester, LE1 7RH, UK.*
[2]*Chief Scientist's Directorate, Natural England, 8 City Walk, Leeds, LS11 9AT, UK.*
[3]*State Key Laboratory of Palaeobiology and Stratigraphy, Nanjing Institute of Geology and Palaeontology, Chinese Academy of Sciences, Beijing East Road 39, 210008 Nanjing, China*
[4]*Biogéosciences, UMR 6282 CNRS, Université de Bourgogne, 6 Boulevard Gabriel, 21000 Dijon, France.*
[5]*Department of Earth Sciences, Downing Street, University of Cambridge, Cambridge, CB2 3EQ, UK.*

## ABSTRACT

Climate change is demonstrably linked to radiations, extinctions, and turnovers in the biosphere throughout the Phanerozoic (538.8 Ma to present). Here, we show that this connection existed as far back as the late Ediacaran (~579 to 538.8 Ma), the first interval in Earth's history to host complex macroscopic organisms including early animals. To do this, we systematically evaluate the dating, correlation, and likely glaciogenicity of candidate Ediacaran glaciogenic deposits to produce a first-order climatic framework for the mid- to late Ediacaran. In contrast to previous studies, our systematic approach accounts for uncertainties in chronostratigraphy, correlation, and depositional interpretation of candidate glaciogenic deposits. Through this systematic approach we reduce the error envelopes which have allowed previous interpretations of either one long (>20 Myr) or up to four short (1 to 5 Myr) ice ages during the mid- to late Ediacaran. We show that the available data support two intervals of icehouse climate state (mid-Ediacaran, ~593 to 579 Ma; and late Ediacaran, ~565 to ~550 Ma) that alternated with greenhouse climates (late Ediacaran, ~579 to 565 Ma; and terminal Ediacaran, ~550 Ma to Cambrian). Both icehouse intervals were characterized by geographically restricted glaciations of ~10 to 15 Myr duration, with expansion and retreat of ice sheets. These changes in climate state correspond in time with apparent step-changes in the late Ediacaran biosphere, including to the standing diversity and taxonomic composition of paleocommunities. Our results support a Phanerozoic-style coupling of global climate and biosphere during the early stages of animal evolution.

## INTRODUCTION

Changes in Earth's climate and biosphere are closely linked throughout the Phanerozoic Eon (the last ~539 million years). Transitions between globally cooler and warmer conditions are implicated in extinctions, diversifications, and biotic turnovers in the Phanerozoic fossil record (e.g. Erwin, 2009; Bond and Grasby, 2017; Fenton et al., 2023; Woodhouse et al., 2023). However, it is unclear whether such relationships existed in Earth's earliest known metazoan biosphere, that of the late Ediacaran Period (~580 to 538.8 Ma). The Ediacaran Period follows the Cryogenian Period, which is supposedly characterized by extreme and long-lasting 'snowball' climate conditions (e.g. Hoffman et al., 2017), and precedes the prolonged greenhouse climate of the Cambrian Period (Scotese et al., 2021; Wong Hearing et al., 2021). The Ediacaran Period can therefore be viewed as a transitional interval in Earth's climate history, coincident with the early diversification of animals and reorganization of the carbon cycle (Butterfield, 2009; Wood et al., 2019; Xiao and Narbonne, 2020).

Evidence for glaciogenic sedimentary deposits of broadly mid- to late Ediacaran age has been widely recognized in the rock record, and candidate glacial deposits have been variously considered to represent either several very short glaciations (e.g. Pu et al., 2016; Retallack, 2022; Linnemann et al., 2022; Niu et al., 2024) or one continuous 20 to 40 million year icehouse interval with a shifting locus (e.g. Wang et al., 2023a, 2023b). These studies all propose testable hypotheses of a first-order climatic framework for the mid- to late Ediacaran Period. Testing these hypotheses requires a systematic consideration of the depositional ages and genesis of the rocks on which they rest. However, recent compilations of candidate Ediacaran glacial units have applied inconsistent criteria to assemble only partially overlapping subsets of deposits (Figure 1) within different correlation frameworks (Table 1; Figure S1; Youbi *et al.* 2020; Retallack 2022; Wang *et al.* 2023a, b; Niu *et al.* 2024). The resulting uncertainty about which deposits are glacial and how they should be correlated has hindered assessments of Earth's climate evolution through this critical interval in biosphere evolution. It remains unclear, for example, whether the largest carbon cycle perturbation in the geological record, the Shuram excursion with $\delta^{13}C$ values as low as –12 ‰, occurred when Earth was in a greenhouse (Shields et al., 2019; Bergmann et al., 2022) or an icehouse (Wang et al., 2023a, 2023b) climate state.

Here, we build on recent advances in stratigraphic correlation (e.g. Rooney et al., 2020; Yang et al., 2021; Busch et al., 2023; Bowyer et al., 2023, 2024) and paleobiology (e.g. Boag et al., 2016, 2024; Muscente et al., 2019; Boddy et al., 2021; Surprenant and Droser, 2024; Bowyer et al.,

2024) to interrogate the co-evolution of physical and biological components of the Earth System through the Ediacaran Period. Specifically, we combine sedimentological and paleobiological data in a refined chronostratigraphic framework to evaluate the hypothesis that there is a temporal link between global climate state and biodiversity dynamics (faunal turnovers) in the late Ediacaran geological record.

Extrapolating from the Phanerozoic Earth System, we would expect to see in the fossil record a biosphere response to changing climate via changes in standing diversity and/or taxonomic composition (e.g. Erwin, 2009; Woodhouse et al., 2023). The absence of this pattern in the Ediacaran (the null hypothesis) would indicate (a) that geological and collection biases currently obscure our ability to read the Ediacaran geological record, and/or (b) that our data have insufficient age controls for accurate correlation, and/or (c) that the Ediacaran biosphere had a fundamentally different relationship to the climate system than the Phanerozoic biosphere.

Understanding past temporal relationships between the biosphere and climate system is essential for evaluating hypotheses of how animal evolution affected Earth's climate evolution, and *vice versa*.

## MATERIALS AND METHODS

### Ediacaran glacial deposits

We distinguish between icehouse and greenhouse climate states by the presence or absence of low altitude continental ice sheets respectively (e.g. Macdonald et al., 2019), and note that the presence of sea ice alone is insufficient evidence of icehouse conditions.

Uniquely, we performed a systematic assessment of both the dating and sedimentological evidence for candidate mid- to late Ediacaran glaciogenic deposits. Although most recent workers have considered the dating evidence for candidate Ediacaran glaciogenic deposits, they have not systematically considered the sedimentological evidence that each deposit was actually formed by ice-related processes, i.e. the likely glaciogenicity (Table 1; Figure 1). Here, we have explicitly and systematically considered the sedimentological evidence for each candidate Ediacaran glaciogenic deposit following the star rating system of Tindal (2023) and which is outlined below (Table 2; Supplementary Data 1).

Our dataset (Supplementary Data 1) is derived from the compilations of Youbi et al. (2020), Retallack (2022), Tindal (2023), Wang et al. (2023a, b), and Niu et al. (2024), with additional data drawn from references cited in those studies, notably Hambrey and Harland (1981) and Arnaud et al. (2011), as well as more recent publications. All deposits included in the compilations of Youbi et al. (2020), Retallack (2022), Wang et al. (2023a, b), and Niu et al. (2024) were considered here. Deposits not included in these compilations but that were included in Tindal's (2023) Appendix 2 were considered where:

1) their glaciogenicity score was greater than one star (see below; Tindal, 2023), AND
2) an Ediacaran depositional age was plausible, meaning that:
    a) neither age constraint contradicts an Ediacaran age, AND
    b) at most one of the maximum and minimum age constraints is missing (“NA”), AND
        i) the maximum age constraint is not older than 635 Ma, OR
        ii) the minimum age constraint is older than the Ordovician Period (486.85 Ma) AND younger than 600 Ma

(i.e. the maximum age is Ediacaran or the minimum age is mid-Ediacaran to Cambrian).

After this screening process, many of the remaining deposits from Tindal (2023) are still more likely of Cryogenian than Ediacaran age, based on non-radiometric constraints.

***Determining depositional age***

There is substantial circularity in the dating and correlation of Neoproterozoic putative glaciogenic deposits (Tindal, 2023), which is partly responsible for the discrepancies between previous compilations (Table 1; Table 3; Figure 1). Putative Neoproterozoic glaciogenic deposits tend to be correlated together on lithostratigraphic grounds ('glaciostratigraphy'; Tindal 2023). Independent age constraints are therefore crucial for testing potential patterns and quantifying temporal uncertainty in global paleoclimate data.

Literature searches were performed to make rigorous assessments of depositional age for each potentially glaciogenic deposit. Where available, radiometric age constraints are preferred. Radiometric dates were included only if they possess a well-documented stratigraphic relationship with a putative glaciogenic deposit. Chemostratigraphic evidence is considered where there is good evidence for regional and global chemostratigraphic correlation. Biostratigraphic age constraints are a valuable but uncertain independent dating method for candidate glaciogenic deposits. In particular, biostratigraphy is useful where Cambrian or Ediacaran fossils are found overlying a diamictite deposit. For example in northern China, Arabia, and the Baltic region, where the strata overlying diamictite units contain fossils like *Shaanxilithes* that are known to be restricted to the terminal Ediacaran or older (~550 to 538.8 Ma; Vickers-Rich et al., 2013; Wang et al., 2021b; Agić et al., 2024). Here, where we use late Ediacaran macrofossils to provide an age constraint, we assumed that these taxa could extend up to the Ediacaran–Cambrian boundary and we therefore apply a numerical age constraint of 538.8 Ma (Cohen et al., 2013; Linnemann et al., 2019), though it is likely that the true age constraint is older than this.

***Assessing glaciogenicity***

Putative glaciogenic deposits readily enter the literature, but are very difficult to excise from it if originally misinterpreted, as shown by the number of low-scoring deposits and the variable range of deposits included in or excluded from previous Ediacaran compilations (Table 1; Table 3; Figure 1; Tindal 2023). Neoproterozoic diamictite deposits are frequently interpreted as glaciogenic even when the sedimentology and geotectonic context make a non-glacial origin more parsimonious (e.g. Kennedy et al., 2019; Kennedy and Eyles, 2021; Molén, 2023; Kühnemann et al., 2024; Palacios, 2024; Meinhold et al., 2025). To mitigate for this, we followed the glaciogenicity assessments of Tindal (2023), who devised a semi-quantitative five-star rating scheme to assess the strength of evidence for glaciogenicity of deposits, and applied it consistently across the pre-Pleistocene glacial record.

Tindal's (2023) scheme weights individual lines of sedimentological and geomorphological evidence alongside consideration of the depositional and tectonic context on a geometric progression scale from one to five, where a rating of five indicates unequivocal evidence for glaciation, and a rating of one means that a broad range of ice-free depositional processes could be responsible for producing the assembled characteristics (Table 2; Supplementary Information). The summary rating for each deposit is the weighted sum of all individual depositional characteristics, such that two lines of evidence at one level equate to one line of evidence at the next (higher) level. Because the scoring system incorporates multiple lines of evidence of varying individual strengths, it should be used to guide interpretations of the potentially glacial origins of a deposit but not as a strict diagnostic test.

We consider unreliable those deposits that score less than three out of five stars, meaning that plausibly glaciogenic deposits have ‘circumstantial’ or better evidence that they were formed under glacial influence (Tindal, 2023, tbl. 2.1). For some deposits rated less than three stars, it may be that the level of described evidence does not accurately reflect the evidence that is available in the field, and so they may be upgraded in the future when further data come to light. Where a deposit was not originally rated by Tindal (2023) and/or where substantial new evidence has been published since his initial assessment, author BHT has reviewed the currently available evidence and provided updated ratings for these deposits (Supplementary Information; Supplementary Data 1).

**Ediacaran paleobiological data**

Our paleobiological dataset is primarily based on the compilations of Boddy et al. (2021) and Bowyer et al. (2024), with additional data from Surprenant and Droser (2024), Muscente et al. (2019), and other primary sources (Supplementary Data 2). The primary age model used to calibrate the paleobiology dataset is Bowyer et al.'s (2023, 2024) age model K; for deposits older than ~550 Ma this age model follows Yang et al. (2021); for Mistaken Point Ecological Reserve (MPER) data, we follow the original age model of Matthews et al. (2020). Where further radiometric or carbon isotope age controls are available, these have also been included within an updated age model (Supplementary Data 2).

We follow Wood et al. (2023) in considering each late Ediacaran biotic assemblage to be characterized by the novel morphotypes or major groups that first appear in that assemblage (Supplementary Data 2). For example, this makes the rangeomorph *Rangea* a component of the Avalon assemblage because rangeomorphs first appeared as a key part of the Avalon assemblage, even though *Rangea* itself is only known from deposits younger than ~557 Ma.

Paleobiodiversity analyses were performed in R (R Core Team, 2021) using the package divDyn (Kocsis et al., 2019). We examined raw genus richness and subsampled genus richness using inexact Shareholder Quorum subsampling (SQS; Alroy 2010a, 2014) with a quota of 0.4, unweighted collection-based classical rarefaction (UW) with a quota of eight collections, and occurrence-weighted by-list subsampling (OW) with a quota of 14 occurrences.

The depositional age of the classic White Sea assemblage fossils from South Australia (East Gondwana) is only loosely constrained by the ~566 Ma Shuram-correlative Wonoka Formation negative CIE below (Yang et al., 2021; Busch et al., 2022, 2023) and the Terreneuvian (early Cambrian) Uratanna and Parachilna formations above (Betts et al., 2018). The Ediacara Member fossiliferous deposits are typically correlated on the basis of taxonomic similarity with the better constrained deposits of the White Sea region of the East European Platform (Waggoner, 2003; Boag et al., 2016; Muscente et al., 2019; Boddy et al., 2021; Bowyer et al., 2022, 2023, 2024; Evans et al., 2022). We performed our paleontological analyses using the full dataset, and then performed sensitivity analyses on the dataset excluding South Australia occurrences to understand the impact of the lack of precise dating of these sections.

**RESULTS**

Recent publications that compile, compare, or review candidate Ediacaran glaciogenic deposits (Table 1) can be grouped into three broad categories (Figure S1): (a) those that correlate most glacial evidence to the Gaskiers glaciation (~580 Ma; Youbi et al. 2020), (b) those that argue for two to four short-lived (~1 to 5 Myr) glaciations (Linnemann et al., 2018, 2022; Retallack, 2022; Niu et al., 2024), and (c) those that argue for a single, protracted, late Ediacaran icehouse of ~20 to 40 Myr duration (Wang et al., 2023a, 2023b). Figure 2 shows our updated compilation of candidate mid- to late Ediacaran glaciogenic deposits and our assessment of the strength of evidence for their glaciogenicity. The most parsimonious interpretation of our data identifies two icehouse intervals of 10 to 15 Myr in duration, here termed the mid-Ediacaran icehouse (MEIH; ~593 to 579 Ma) and the late Ediacaran icehouse (LEIH; ~565 to 550 Ma), separated by greenhouse intervals termed the late Ediacaran greenhouse (LEGH; ~579 to 565 Ma), and the terminal Ediacaran greenhouse (TEGH; ~550 Ma to Cambrian).

**593 to 579 Ma: mid-Ediacaran icehouse (MEIH)**

Our compilation demonstrates that there is strong support for Earth's climate being in an icehouse state in the mid-Ediacaran between ~593 to 579 Ma (Figure 2), even when deposits with low confidence of a glaciogenic interpretation (less than three stars) are discounted. This icehouse was previously considered to be a short-lived cold interval of perhaps less than 1 Myr, characterized as the 'Gaskiers glaciation' at ~580 Ma (Pu et al., 2016). There is now evidence for icehouse conditions lasting perhaps ~5 Myr on Avalonia (Fitzgerald et al., 2024; Mills et al., 2024), ~10 Myr on the Rio de Plata craton (Oyhantçabal et al., 2007; Mallmann et al., 2007), and ~10 to 15 Myr on North African Gondwana (Letsch et al., 2018), with a consistent termination age of ~579 Ma (Figure 2). Often called the 'Gaskiers glaciation', here we use the term 'mid-Ediacaran icehouse' (MEIH) to emphasize its broader paleogeographical and temporal distribution (Figure 2).

Of the deposits identified in this interval, the Gaskiers Formation and Trinity diamictite (Avalonia; eastern Newfoundland, Canada), both rated four star deposits (Tindal, 2023), have the tightest age constraints for the termination of glacial activity. Underlying the Gaskiers Formation in eastern Newfoundland, the Mall Bay Formation is only rated a two star deposit (Supplementary Information) but indicates evidence of cold conditions on Avalonia prior to deposition of the Gaskiers and Trinity diamictites (Fitzgerald et al., 2024). Overlying the

Gaskiers Formation, turbidites of the Drook Formation were deposited in similar deep water slope settings and contain some of the oldest Ediacaran macrofossils (Matthews et al., 2020), but appear to lack evidence of glacial influence. This is despite much paleontological and stratigraphical research on the upper part of this unit (Hofmann et al., 2008; Matthews et al., 2020), and may indicate a sharp change in the local climate regime at ~579 Ma (Pu et al., 2016). Strata of the lower Drook Formation may offer insights into the climatic transition at the end of the MEIH. The Squantum Member diamictite, Roxbury Conglomerate Formation (Avalonia; northeast USA), has been radiometrically constrained to between ~595 to 570 Ma (Thompson and Bowring, 2000; Thompson et al., 2007). Although rated a four star deposit (Tindal, 2023), the reliability of reports of striated clasts has been called into question, with some studies concluding there is no strong evidence of glaciogenicity (Dott 1961; Socci and Smith 1990; Carto and Eyles 2012; Supplementary Information). Nevertheless, the glaciomarine Gaskiers and Trinity diamictites provide strong positive evidence for low altitude glaciation on Avalonia, terminating at ~579 Ma.

Candidate glaciogenic deposits in the Tiddiline Group and Izdar Member (West Gondwana; Morocco), both rated three star units (Tindal, 2023), were deposited between ~593 to 579 Ma (Thomas et al., 2002; Inglis et al., 2004; Blein et al., 2014; Letsch et al., 2018). The diamictites are interpreted as both terrestrial and marine tillites, providing evidence for proximal glacial activity, whereas the laminites with dropstones reflect more distal glaciomarine conditions (Letsch et al., 2018). The repeated alternation of tillites and laminites evidences local waxing and waning of low altitude land ice on West Gondwana (Letsch et al., 2018).

The Las Ventanas and Playa Hermosa formations (Río de Plata craton; southern Uruguay) are both rated three star deposits (Tindal, 2023). The Las Ventanas Formation is constrained by radiometric dates to between 590 ± 2 Ma to 579 ± 1.5 Ma (Oyhantçabal et al., 2007; Mallmann et al., 2007), consistent with less precise radiometric ages and acritarch biostratigraphy (Bossi et al., 1993; Sanchez Bettucci and Linares, 1996; Gaucher et al., 2008; Pecoits et al., 2011). The Playa Hermosa Formation is radiometrically constrained to between 594 ± 16 Ma and 578.0 ± 4.3 Ma (Rapalini et al., 2015). The Las Ventanas and Playa Hermosa formations were deposited in a tectonically active setting with evidence of non-glaciogenic debris flow deposits, but the candidate glaciogenic deposits include diamictites and fine-grained rhythmites hosting outsized clasts with facetted surfaces (Pecoits, 2003; Pecoits et al., 2008, 2011; Gaucher et al., 2008; Pazos et al., 2011).

The Tany, Koyva, and Starye Pechi formation diamictites of the Serebryanka and Sylvitsa groups (Baltica; central Urals, Russia) are constrained between volcanic zircon U-Pb dates 598.1 ± 6.0 Ma (lower Tany Formation) and 567.2 ± 3.9 Ma (the overlying Perevalok Formation; Chumakov, 2011; Grazhdankin et al., 2011; Maslov et al., 2013; Chumakov et al., 2013). The Tany, Koyva, and Starye Pechi diamictites are variously interbedded with shales and massive quartz-feldspar sandstones as well as minor carbonates (Grazhdankin et al., 2009; Chumakov, 2011). The geological context indicates deposition on an outer shelf to slope setting, with the diamictites interbedded with various gravity-driven mass flow-derived deposits including flysch, conglomerates, breccias, turbidites, and syn-sedimentary slumping (Chumakov, 2011; Maslov et al., 2013; Chumakov et al., 2013). All three units are reported to have evidence indicating a glaciogenic origin including rare (Ipat'eva *in* Maslov et al., 2013) striated and outsized clasts, and are rated four (Tany) and three (Koyva, Starye Pechi) star deposits (Tindal, 2023). It is possible, though unproven, that the Starye Pechi Formation was deposited after the MEIH, in the LEGH (see below).

**579 to 565 Ma: late Ediacaran greenhouse (LEGH)**

The late Ediacaran experienced a major perturbation to the carbon cycle, as recorded by the Shuram negative CIE (Xiao and Narbonne, 2020; Yang et al., 2021; Busch et al., 2022), which began no earlier than 575 Ma (Rooney et al., 2020; Yang et al., 2021) and terminated after 566.9 ± 3.5 Ma (Busch et al., 2023). The Shuram CIE has been studied in globally distributed sections and a wide range of depositional settings (e.g. Yang et al., 2021; Busch et al., 2022; Bergmann et al., 2022; Cantine et al., 2024), yet there are no currently known sections in which a Shuram-like CIE is coincident with a candidate glaciogenic deposit.

However, carbonate olistoliths from the Kernos, Buton, and Starye Pechi formations have yielded very negative (–10 to –15 ‰) carbon isotope values that were originally interpreted as either diagenetic or resulting from methane or carbon dioxide seeps (Chumakov et al., 2013). We suggest that an alternative interpretation is that these carbon isotope values reflect deposition of the olistolith source material during the Shuram CIE. In combination with the 567.2 ± 3.9 Ma radiometric minimum depositional age constraint on the Starye Pechi Formation (Grazhdankin et al., 2011), the olistolith carbon isotope data could provide a depositional window of ~574 to 567 Ma for the Starye Pechi diamictites. If the original interpretation (Chumakov et al., 2013) of the very negative carbon isotope values is correct, the Starye Pechi Formation may predate the Shuram CIE and be contemporaneous with the MEIH. On current evidence, we consider that both pre-Shuram (MEIH) and syn-Shuram (LEGH) age assignments are plausible, and that further evidence is needed to resolve this question.

There are no further candidate glaciogenic deposits with reasonable depositional age constraints that could plausibly have been deposited between ~579 to 565 Ma (Figure 2). In sections with near-continuous sedimentation, there is no evidence for glaciation after ~579 Ma and before ~565 Ma, including in Avalonian sections where glacial deposits were well developed prior to ~579 Ma and there is no substantial change in depositional setting (Carto and Eyles, 2011; Pu et al., 2016; Fitzgerald et al., 2024; Mills et al., 2024). Because of the lack of well-constrained evidence for glaciation, we term this interval the 'late Ediacaran greenhouse' (LEGH).

**565 to 550 Ma: late Ediacaran icehouse (LEIH)**

At around ~565 to 560 Ma, a concentration of evidence for land ice returns (Figure 2) on Gondwana and peri-Gondwanan terranes (Linnemann et al., 2018, 2022). This icehouse interval has been known by various names, but particularly as the 'Hankalchough glaciation', or the 'Upper Ediacaran Glacial Period' (Linnemann et al., 2022). Here, we use the term 'late Ediacaran icehouse' (LEIH) for consistency of terminology and to avoid tying the climate interval to specific deposits.

The Ouarzazate Group diamictites and glacial surfaces (West Gondwana; Morocco) are rated a four star deposit (Supplementary Information), with a maximum depositional age of 566 ± 4 Ma (Blein et al., 2014), therefore likely post-dating the recovery of the Shuram CIE. The Kahar Formation diamictite (East Gondwana; Iran), rated a three star deposit (Tindal, 2023), has a radiometrically constrained maximum depositional age of 563.1 ± 3.9 Ma and a formal minimum age of 538.8 Ma informed by overlying earliest Cambrian trace fossils (Etemad-Saeed et al., 2016). The Kahar diamictite has also been suggested to be older than 550.3 ± 3.6 Ma based on the younger age population of detrital zircons in an overlying sample (Etemad-Saeed et al., 2016). The Dhaiqa Formation diamictite (East Gondwana; Saudi Arabia), rated a three star deposit (Tindal, 2023), is younger than 560 ± 4 Ma and underlies candidate Ediacaran fossils (Miller et al., 2008; Vickers-Rich et al., 2013).

Several candidate glaciogenic deposits in the paleo-terranes of present-day northern China have poor age constraints but were likely deposited between ~565 to 550 Ma (Xiao et al., 2004; Shen et al., 2007, 2010; Zhou et al., 2019; Le Heron et al., 2019; Wang et al., 2021b, 2023b). The Luoquan and Zhengmuguan formations (North China Craton; China) are four star (Tindal, 2023) and three star (Supplementary Information) deposits, respectively. The Luoquan and Zhengmuguan formations are likely correlatives (Le Heron et al., 2019; Wang et al., 2021b) and were deposited below the first occurrences of the late Ediacaran tubular taxon *Shaanxilithes* in the conformably overlying Dongpo and Tuerkeng formations respectively (Shen et al., 2007; Zhou et al., 2019; Wang et al., 2021b). Similarly, the poorly documented Hongtiegou Formation diamictite (Qaidam Block; China; Supplementary Information) was deposited below occurrences of *Charnia* and *Shaanxilithes* in the Zhoujieshan Formation (Shen et al., 2010; Pang et al., 2021; Wang et al., 2022). The Luoquan, Zhengmuguan, and Hongtiegou formations unconformably overlie Mesoproterozoic sedimentary deposits but are conformable with their overlying, Ediacaran fossil-bearing, units (Shen et al., 2007, 2010; Wang et al., 2021b). The Hankalchough Formation (Tarim Block; China) is a three star deposit (Supplementary Information) and occurs at least 65 m stratigraphically above the recovery limb of an extreme negative CIE in the Shuiquan Formation that has been correlated with the Shuram CIE (Xiao et al., 2004; Wang et al., 2023a). The maximum depositional age of the Hankalchough Formation is therefore taken as the minimum age of the Shuram CIE recovery: 566.9 ± 3.5 Ma (Busch et al., 2023). The overlying Xishanblaq Formation hosts earliest Cambrian acritarchs, which provide a minimum age constraint on the Hankalchough Formation (Xiao et al., 2004; Yao et al., 2005).

The Mortensnes Formation diamictite (Baltica; Norway) is a three star deposit (Tindal, 2023) lacking precise radiometric dates, but it is also constrained by a likely Shuram-equivalent CIE below (Halverson et al., 2005; Rice et al., 2011) and Ediacaran macrofossils above (Högström et al., 2013; McIlroy and Brasier, 2017; Jensen et al., 2018; Agić et al., 2024). It is likely that the Mortensnes Formation was deposited between the Shuram CIE and the terminal Ediacaran.

Four candidate glaciogenic deposits have been identified across the peri-Gondwanan Cadomia microcontinent (Linnemann et al., 2018, 2022). Diamictites from the Müglitz Formation (Weesenstein Group) and Clanschwitz Group Member 3 (both Cadomia; Germany) are rated two and one star deposits respectively (Supplementary Information) and were considered to be likely younger than 562 ± 5 Ma (Linnemann et al., 2018). However, recent work has indicated a non-glacial origin for these units as well as a considerably revised depositional age of late Cambrian to Ordovician based on U-Th-Pb monazite dates (Kühnemann et al., 2024) and ichnofossil evidence (Meinhold et al., 2025). The Granville Formation diamictites (Cadomia; France), rated a three star deposit (Tindal, 2023), are younger than 562.1 ± 3.1 Ma, with the upper diamictite younger than 560.6 ± 3.3 Ma (Linnemann et al., 2022). The Orellana Formation (Cadomia; Spain), rated a two star deposit (Tindal, 2023) and not universally regarded as glaciogenic (Palacios, 2024), is younger than 565 ± 4 Ma (Linnemann et al., 2018) and is found unconformably below late Ediacaran fossil-bearing carbonates (Álvaro et al., 2019; Palacios, 2024). Overall, the evidence for late Ediacaran glaciation across Cadomia in the ~565 to 550 Ma interval is weak in comparison to that on paleocontinental Gondwana and the terranes of northern China.

Where there is depositional continuity above the LEIH candidate glaciogenic deposits, Ediacaran fossils are commonly found in the overlying strata (Shen et al., 2007, 2010; Högström et al., 2013; Vickers-Rich et al., 2013; Jensen et al., 2018; Wang et al., 2021b, 2022; Agić et al., 2024), demonstrating that this icehouse terminated before the end of the Ediacaran. Less well constrained than the MEIH, the LEIH probably commenced after the Shuram CIE recovery, likely between 565 to 560 Ma, and terminated before the end of the Ediacaran Period, likely about ~550 Ma (Xiao et al., 2004; Miller et al., 2008; Chumakov, 2009; Vickers-Rich et al., 2013; Etemad-Saeed et al., 2016; Linnemann et al., 2018, 2022; Agić et al., 2024).

**550 to 539 Ma: terminal Ediacaran greenhouse (TEGH)**

There is scant evidence of glaciation in the terminal Ediacaran, likely after ~550 Ma. The only temporally well-constrained candidate glaciogenic deposit known from this interval is the Vingerbreek Member of the Nudaus Formation, Nama Group (Kalahari Craton; East Gondwana; Namibia and South Africa) and the associated basal Vingerbreek Unconformity (Schwellnus, 1941; Kröner and Germs, 1971; Kröner, 1981; Germs and Gaucher, 2012; Zieger-Hofmann et al., 2022), which are together rated as a three star unit (Tindal, 2023). The Vingerbreek Member and Unconformity are radiometrically constrained to between 547.36 ± 0.23 Ma (Bowring et al., 2007) to 545.27 ± 0.11 Ma (Nelson et al., 2022).

The Vingerbreek Unconformity has only been found in parts of the southern Nama Basin (the Zaris and possibly the Vioolsdrif sub-basins), not in the Witputs sub-basin to the north (Kröner, 1981; Germs and Gaucher, 2012; Zieger-Hofmann et al., 2022). The Vingerbreek Member basal diamictite was deposited in wide channels in the unconformity surface, which have been interpreted as deriving from fluvial or submarine mass flow erosion processes; both far-field glacioeustasy and tectonism have been proposed as potentially responsible for lowering base level (Martin, 1965; Kröner, 1981; Germs and Gaucher, 2012). The grooves and surface polish on some channel flanks have been interpreted as deriving from glacier-rock (Schwellnus, 1941; Germs and Gaucher, 2012; Zieger-Hofmann et al., 2022) or sea ice-rock (Martin, 1965; Kröner, 1981) interactions, though similar features also form from mass flow and rock avalanche erosion processes (Hambrey and Harland, 1981; Hu and McSaveney, 2018). The diamictite deposits are better described as conglomerates and breccias (Germs and Gaucher, 2012) and have been interpreted as fluvial or submarine current-derived deposits, including in studies that found glacial action at least partly responsible for the unconformity (Kröner, 1981; Germs and Gaucher, 2012). In northwest South Africa, the diamictite grades into turbidites (Zieger-Hofmann et al., 2022). The Vingerbreek Member and Unconformity therefore provide only circumstantial, stratigraphically and spatially isolated evidence for glacial ice. Further field work is required to determine the depositional context of the Vingerbreek Unconformity and Vingerbreek Member, and it stands as a test of our hypothesis that the ~550 to 545 Ma interval was characterized by a greenhouse climate.

Elsewhere the terminal Ediacaran lacks any signs of glaciation, and we therefore use the term 'terminal Ediacaran greenhouse' (TEGH) for this interval. Similar to previous compilations of climatically sensitive lithologies (Boucot et al., 2013; Wong Hearing et al., 2021), we do not find evidence of well-dated glacial sedimentary deposits in either the terminal Ediacaran or early Cambrian periods.

**Climate and the Ediacaran biosphere**

Our analysis indicates that the mid- to late Ediacaran climate was characterized by two icehouse intervals (~593 to 579 Ma and ~565 to 550 Ma) and two greenhouse intervals (~579 to 565 Ma and ~550 to 539 Ma). Independent of our analysis, the late Ediacaran biosphere has been characterized by three distinct marine biotic assemblages (Figure 3; Figure 4; Table 4), governed by some combination of environmental and evolutionary controls (Waggoner, 2003; Grazhdankin, 2004; Gehling and Droser, 2013; Boag et al., 2016; Muscente et al., 2019; Evans et al., 2022). To test whether biotic turnover is coincident with climatic shifts, we examine diversity dynamics over this interval, mindful that the assemblages are typically found in different paleogeographic regions and depositional settings, as well as time intervals (Waggoner, 2003; Boag et al., 2016, 2024; Muscente et al., 2019; Boddy et al., 2021; Bowyer et al., 2022, 2024; Evans et al., 2022). Because of the substantial contribution of geological and societal biases in the current Ediacaran fossil record (taxonomic richness largely follows sampling intensity; Figure 5; Bowyer *et al.* 2024), it is generally more instructive to consider taxonomic composition than taxonomic richness. Nevertheless, some biodiversity signals do appear to be robust to sampling biases (Figure 5).

***The Avalon biotic assemblage***

Diverse communities of the Ediacaran macrobiota, belonging to the Avalon biotic assemblage, first appear in deep marine siliciclastic deposits between ~579 to 575 Ma (Figure 4), after the MEIH and before the Shuram CIE (Pu et al., 2016; Matthews et al., 2020; Yang et al., 2021; Boag et al., 2024; Bowyer et al., 2024). The Avalon biotic assemblage comprises predominantly sessile benthic taxa including frondose and non-frondose morphologies, some of which likely stood up in the water column whereas others reclined on the sea floor (Gehling and Narbonne, 2007), alongside candidate cnidarians (e.g. Liu et al., 2014a, 2015; Dunn et al., 2022), and rare trace fossils (Liu et al., 2010, 2014b). This assemblage reaches an apparent acme in diversity in deep marine settings around 565 Ma (Matthews et al., 2020; Boag et al., 2024), coincident with the end of the LEGH and the transition into the LEIH (Figure 4). The Avalon biotic assemblage persists in deep water settings until at least 560 Ma (Wilby et al., 2011; Noble et al., 2015; Kenchington et al., 2018). The post-560 Ma fate of the deep water Ediacaran biota remains unknown due to the scarcity of deep marine siliciclastic deposits after this time (Bowyer et al., 2024).

Depauperate communities of the Avalon biotic assemblage are known from shallow marine settings on Avalonia (Cope, 1977, 1983; Gehling et al., 2000; Menon et al., 2013; Menon, 2015; Hawco et al., 2021) and Laurentia (Hofmann et al., 1983; Narbonne and Hofmann, 1987; Pyle et al., 2004; Moynihan et al., 2019) after, but not before or during, the Shuram CIE (~574 to 566 Ma; Matthews et al., 2020; Boag et al., 2024; Clarke et al., 2024). The post-Shuram CIE shallow marine Avalon biotic assemblages are differentiated from the shallow marine White Sea biotic assemblages more by the absence of taxa rather than their presence. There are no taxa exclusive to the Avalon biotic assemblage in these shallow water deposits. The tubular fossils, dickinsoniomorphs, bilaterialomorphs, and radial morphogroups that are ubiquitous in younger White Sea biotic assemblage deposits are absent from the shallow marine Avalon biotic assemblage sites, as well as from coeval post-Shuram deeper marine sites (Narbonne et al., 2014; Noble et al., 2015; Carbone et al., 2015; Kenchington et al., 2018; Boag et al., 2024; Clarke et al., 2024).

The low number and diversity of shallow water occurrences of the Avalon biotic assemblage may be an artefact of environmental specificity, preservation, or collection bias, but it is notable that no macrofossils have been recovered from pre-Shuram CIE shallow marine rocks with suitable sedimentology for fossil preservation and that have been intensively studied (Boag et al., 2024). Although the scarcity of deep marine siliciclastic deposits after ~560 Ma may explain the apparent loss of the deep water Avalon biotic assemblage, there is no concomitant absence of pre- and syn-Shuram CIE shallow and mid-depth marine carbonate and siliciclastic deposits (Bowyer et al., 2024); i.e. there are older strata which could have preserved a shallow marine Avalon biotic assemblage if it was present (such as the shallow marine facies of the Nadaleen and Gametrail formations, NW Canada; Boag et al., 2024). This observation lends support to the idea that the majority of Avalon assemblage taxa belonged to a deep-water biotope (Boag et al., 2016, 2024; Bowyer et al., 2024), with some components (e.g. *Charnia* and *Charniodiscus*) being environmentally tolerant generalist taxa that were capable of inhabiting shallower marine settings in the later Ediacaran (Grazhdankin, 2014; Boag et al., 2024). Here we suggest that a ~565 to 560 Ma interval of global cooling at the onset of the LEIH allowed more generalist taxa of the otherwise deep water adapted Avalon assemblage to colonize cooling shallow marine environments.

***The White Sea biotic assemblage***

*In situ* paleocommunities of White Sea biotic assemblage taxa are found in shallow marine settings, above storm weather wave base and predominantly above fair weather wave base (e.g. Grazhdankin, 2004; McMahon et al., 2020) from before 557 Ma until at least 553 Ma (Martin et al., 2000; Fedonkin et al., 2012; Grazhdankin, 2014; Yang et al., 2021; Bowyer et al., 2022, 2024). Our analysis places this range within the LEIH. The White Sea biotic assemblage is defined by the appearance of new morphogroups, including bilaterialomorphs, radialomorphs, and tubular forms, which occur alongside a few persistent Avalon-type taxa (Figure 4; Table 4; Martin *et al.* 2000; Narbonne 2005; Fedonkin *et al.* 2012; Grazhdankin 2014; Muscente *et al.* 2019; Surprenant and Droser 2024). The first step-change in trace fossil diversity is associated with this interval – rare trace fossils older than 560 Ma are stratigraphically isolated simple surface traces (Liu et al., 2010, 2014b), but from at least 557 Ma a range of horizontal burrows and trails created by candidate bilaterians are found in shallow marine deposits (Figure S2). Novel morphogroups are found in shallow marine strata deposited during the latter part of the LEIH (~560 to 550 Ma) but not before ~560 Ma (see above; Boag et al., 2024; Clarke et al., 2024). By raw taxonomic richness, the White Sea is the most diverse of the three biotic assemblages and, although the Ediacaran fossil record is strongly affected by sampling biases, the White Sea diversity peak may be robust to some subsampling methods designed to mitigate such biases (Figure 5), and is robust to the inclusion and exclusion of data from South Australian sites which have only loose age constraints (compare Figure 4 and Figure S3, and Figure 5 and Figure S4).

***The Nama biotic assemblage***

The Nama is the youngest of the three biotic assemblages, and is found in shallow marine carbonate and siliciclastic deposits younger than ~550.5 Ma (Darroch et al., 2015; Muscente et al., 2019; Xiao et al., 2021; Wood et al., 2023; Boag et al., 2024) up to the base of the Cambrian (Linnemann et al., 2019; Bowyer et al., 2022, 2023, 2024; Nelson et al., 2022; Wood et al., 2023; Runnegar et al., 2024). It is characterized by the diversification of trace fossils, particularly vertical burrows, and the appearance of biomineralized tubular taxa, which are found only in deposits younger than ~550.5 Ma (Wood et al., 2023; Surprenant and Droser, 2024). Some White Sea-type taxa, including dickinsoniomorphs and erniettomorphs (Xiao et al., 2021; Wang et al., 2021a; Wood et al., 2023), and Avalon-type taxa, including arboreomorphs and rangeomorphs (Xiao et al., 2021; Wu et al., 2022), are found alongside novel Nama morphogroups in shallow marine deposits from this interval. Recent work has shown that there is a considerable overlap in the depositional settings of major White Sea and Nama biotic assemblage sites, increasing the likelihood that the differences in assemblage composition reflect a biological change rather than a change in the environments being sampled (McMahon et al., 2020; Evans et al., 2022; O'Connell et al., 2024). Under our analysis, the Nama biotic assemblage is coincident with the TEGH.

***Summary***

The Ediacaran macrobiota was initially restricted to deep marine settings during the LEGH (Avalon assemblage, ~575 to 565 Ma; Boag et al., 2024); from the beginning of the LEIH (~565 Ma) elements of the Avalon assemblage appear to have colonized shallow marine settings. The first step-change in high-level taxonomic composition of the Ediacaran biosphere, including the advent of bilaterians and non-mineralized tubes, occurred early in the LEIH (before 557 Ma) with the appearance of White Sea biotic assemblage morphogroups. This step-change is underlined by the Ediacaran peak origination rate across the Avalon-White Sea transition, and the subsequent White Sea peak in taxonomic richness (Figure 5). A second step-change in high-level taxonomic composition accompanied the transition from the LEIH to the TEGH (~550 Ma) with the appearance of biomineralizing taxa and vertical burrowing in shallow marine settings. The majority of taxonomic elements of the Avalon biotic assemblage are not found in the younger White Sea and Nama communities, and similarly the majority of White Sea biotic assemblage taxa are not found in Nama communities (Figure 4; Boag et al., 2016; Muscente et al., 2019; Evans et al., 2022; Wood et al., 2023; Bowyer et al., 2024). Considering only shallow water occurrences (from strata deposited above storm-weather wave base), the small numbers of taxa shared between the shallow water Avalon, White Sea, and Nama communities support discrete episodes of faunal turnover (extinctions and radiations) in the shallow marine realm across the late Ediacaran (Figure 4). There appear to be distinct assemblages of morphogroups in the late Ediacaran (Waggoner, 2003; Boag et al., 2016; Muscente et al., 2019; Evans et al., 2022) that are separated in time, demarcated by the prevailing climate regime.

## DISCUSSION

### The timing of Ediacaran climate change

The glacial sedimentary record provides evidence of low altitude grounded ice for two ~15 Myr intervals in the mid- and late Ediacaran (~593 to 579 Ma and ~565 to 550 Ma; Figure 2). Our analysis, based on a systematic treatment of all so far reported candidate mid- and late Ediacaran glaciogenic deposits, argues against previous hypotheses of either one long (e.g. Wang et al., 2023a, 2023b) or two to four very short (<5 Myr; e.g. Retallack, 2022; Linnemann et al., 2022; Niu et al., 2024) glacial intervals.

The termination of the mid-Ediacaran icehouse (MEIH) is well constrained to ~579 Ma by radiometrically dated deposits in North Africa (Thomas et al., 2002; Inglis et al., 2004; Blein et al., 2014; Letsch et al., 2018; Youbi et al., 2020), the Rio de Plata craton (Oyhantçabal et al., 2007; Mallmann et al., 2007), and Avalonia (Pu et al., 2016; Mills et al., 2024). In Oman, and elsewhere on the paleo-Gondwanan margin, the pre-Shuram CIE interval is characterized by condensed sedimentary successions, with a marked increase in depositional rates between ~580 to 560 Ma (Cantine et al., 2024). On the tropical paleolatitude South China craton, stratigraphically constrained glendonite occurrences (indicative of cool or cold water conditions) in the Doushantuo Formation also indicate cooler ocean temperatures between ~600 to 579 Ma

(Wang et al., 2017, 2020; Zhou et al., 2017), with conditions in the basin changing after ~579 Ma and during the EN3/Shuram CIE (Supplementary Information).

The late Ediacaran icehouse (LEIH) is more loosely temporally constrained than the MEIH. Most candidate glaciogenic deposits of this age are broadly bracketed by radiometric dates or the Shuram CIE below and latest Ediacaran or Cambrian fossils above. However, indirect evidence from the broader geological record also supports a climate state transition before the terminal Ediacaran, likely at ~550 Ma.

From a global rock record compilation, Bowyer et al. (2024) identified declining proportions of carbonate and increasing proportions of silicate rocks by area and volume between ~565 to 550 Ma, culminating in a total absence of carbonate rocks from ~555 to 550 Ma. There is a substantial hiatus in deposition on the South China craton between the uppermost Doushantuo Formation and the lowermost Dengying and Liuchapo formations that is younger than EN3/Shuram CIE recovery (~566 Ma) and older than 550.1 ± 0.6 Ma (Yang et al., 2021), coincident with the global sea level lowstand that reached a nadir at ~550.5 Ma (Bowyer et al., 2024), and coincident with the end of the LEIH identified here. The carbonate-barren ~555 to 550 Ma interval is followed by a marine transgression and increasing contribution of carbonates to the global rock record after ~550 Ma (Bowyer et al., 2024). Segessenman and Peters (2024) identified a contemporaneous approximately two-fold increase in sediment volume flux across Laurentia from ~550.5 Ma, persisting until at least 545 Ma. The marine transgression (Bowyer et al., 2024) and increased sediment flux (Segessenman and Peters, 2024) may therefore reflect eustatic sea level rise driven by melting land ice during the transition from the LEIH to the TEGH, with associated increased weathering intensity and/or the flushing of glacial regolith into the oceans.

Above the ~550.5 Ma lowstand, the next identified global transgressive surface is at the Ediacaran-Cambrian boundary (Bowyer et al., 2024), arguably the best known marine transgression in the stratigraphic record (Peters and Gaines, 2012), though of debated origin (e.g. Keller et al., 2019; Tasistro-Hart and Macdonald, 2023). In light of the emerging climate record through this interval, the lack of reported glaciogenic deposits of terminal Ediacaran (see above) or early Cambrian age (Boucot et al., 2013; Johnson et al., 2019; Wong Hearing et al., 2021; Álvaro et al., 2022) supports a tectono-eustatic rather than glacioeustatic driver for this transgression (e.g. Tasistro-Hart and Macdonald, 2023).

What drove the changes in Ediacaran climate state is an open question. Shields et al. (2019) described how the oxidation of a large oceanic reservoir of dissolved organic carbon (DOC) could lead to elevated $pCO_2$ levels and global temperatures through the Shuram CIE, with a temperature-enhanced silicate weathering feedback drawing down $pCO_2$ after the ocean DOC reservoir was exhausted. This temporally constrained mechanism would account for a Shuram interval greenhouse and post-Shuram cooling over several million years (Shields et al., 2019), as we infer from the Ediacaran glacial sedimentary record. Another potential driver of Ediacaran climate is the Central Iapetus Magmatic Province (CIMP) associated with Rodinian break-up and the opening of the Iapetus Ocean (Youbi et al., 2020). Pulsed emplacement of large quantities of mafic igneous rock drives $pCO_2$ up from volcanic outgassing and then down via the silicate weathering feedback effect (Berner, 2004, 2006; Mills et al., 2019). Whatever the principal drivers of Ediacaran climate, our analysis provides a more tightly constrained framework for evaluating Earth System and biosphere evolution through this interval.

**Coupling of climate and biosphere dynamics**

Our analysis consolidates global evidence for step-changes in the Ediacaran biosphere coincident with changes in climate state at ~579 Ma, ~565 to 560 Ma, and ~550 Ma (Figure 2; Figure 4; Figure 5). Considering more proximate potential drivers of biotic change, Evans et al. (2022) found evidence for abiogenic influence, potentially oxygen availability, on Ediacaran biodiversity patterns, and Boag et al. (2024) related the ecophysiology of Ediacaran organisms to potential global temperature regimes, suggesting that high temperatures may have prevented the colonization of shallow water settings during the Shuram CIE. Bowyer et al. (2024) linked Ediacaran biodiversity dynamics to long-term sea level variation and potentially environmental oxygen availability. We suggest that first-order climate state changes provide a first-order driver for the observed large-scale patterns in sea level variation, oxygen availability, and ocean temperature, with the fossil record documenting the biosphere response.

Sea level change has been implicated in shaping both apparent and real Ediacaran biodiversity dynamics by controlling available habitat space and the preserved rock record (Evans et al., 2022; Bowyer et al., 2024). In the Phanerozoic, marine transgressions and sea level highstands, associated with warmer climate states, increased both shallow marine habitat area and preservation potential of the shallow marine shelf (Hallam and Wignall, 1999; Alroy, 2010b). Conversely, cooler intervals are associated with steeper latitudinal diversity gradients (LDGs) driven by increased thermal niche partitioning in the tropics, whereas warmer intervals are associated with flatter LDGs and lower taxonomic richness (Song et al., 2020; Fenton et al., 2023; Woodhouse et al., 2023). Despite sampling limitations, it is notable that the highest Ediacaran taxonomic richness is found during the LEIH (~560 to 550 Ma; Figure 5), an interval characterized by low rock volume, a marine regression, and a sea level lowstand (Bowyer et al., 2024), in agreement with climatically-driven diversity trends in the Phanerozoic (Song et al., 2020; Fenton et al., 2023; Woodhouse et al., 2023).

Ediacaran biosphere dynamics have been closely associated with ocean oxygenation as well as sea level changes (Evans et al., 2018, 2022; Wood et al., 2019; Bowyer et al., 2024). Because an increase in temperature depresses oxygen solubility but elevates metabolic demand, the combination of temperature and ocean oxygenation is crucial for understanding marine habitability (Deutsch et al., 2015; Penn et al., 2018; Boag et al., 2018; Stockey et al., 2021). In this context, higher temperatures of the LEGH and TEGH intervals would have increased ecological stress by reducing thermal niche partitioning and oxygen availability. A resulting prediction is that generalist organisms with tolerance to low oxygen conditions would fare better during icehouse to greenhouse transitions. (Evans et al., 2022) found a positive correlation between organisms' surface area to volume ratio and survivorship through the White Sea to Nama transition, and speculated that a high surface area to volume ratio would be beneficial to surviving in lower oxygen environments. Our analysis suggests a potential mechanism for environmentally-derived selectivity in the Ediacaran biosphere via global temperature change reflecting icehouse/greenhouse transitions.

We suggest that a ~565 to 560 Ma interval of global cooling at the beginning of the late Ediacaran icehouse made it possible for generalist taxonomic elements of the otherwise deep- and cold-water adapted Avalon biotic assemblage such as *Charnia* and *Charniodiscus* to colonize cooling shallow marine environments (Boag et al., 2024). This is similar to the 'polar emergence' pattern observed in the Antarctic fossil record during late Pliocene and early Pleistocene cooling episodes (Berkman et al., 2004), and the inverse of the present-day response to global heating (e.g. Perry et al., 2005). Cooling temperatures with associated increasing thermal gradients (Song et al., 2020; Fenton et al., 2023; Woodhouse et al., 2023), increasing oxygen availability, and decreasing metabolic oxygen demand (Deutsch et al., 2015; Penn et al., 2018; Boag et al., 2018; Stockey et al., 2021) at the beginning of the LEIH may have increased niche availability across the greenhouse to icehouse transition, similar to the thermally-driven polar diversity pump of the Cenozoic (Clarke and Crame, 1992; Griffiths et al., 2023).

Overall, the close correspondence between changes in Ediacaran paleobiology and paleoclimate supports the hypothesis that coupling of the biosphere and climate was established at least by the late Ediacaran Period. Notably, the radiation of bilaterians appears to occur in shallower water settings during a cold interval, and metazoan biomineralization and deep burrowing seem to coincide with a transition from cold to warm conditions. This coupling is evident in spite of uncertainties in global correlation and the known biases of both rock and fossil records (e.g. Bowyer et al., 2024), suggesting that it was a first-order property of the Ediacaran Earth System, as it is for the Phanerozoic.

## CONCLUSIONS

Mid- to late Ediacaran climate appears to be characterized by two discrete intervals of icehouse conditions (MEIH: ~593 to 579 Ma, and LEIH: ~565 to 550 Ma) and two discrete intervals of greenhouse conditions (LEGH: ~579 to 565 Ma, and TEGH: ~550 Ma into the early Cambrian) (Figure 2). The transitions between these climate states are coincident with turnovers in the biosphere (Figure 4). There is wide scope for further work: the causal mechanisms of these climate changes require greater investigation; the known Ediacaran fossil record is particularly unevenly sampled; and the glacial record requires work to constrain both the depositional ages and potential glaciogenicity of many of its deposits. Nevertheless, there is a clear first-order signal in the mid- to late Ediacaran rock record of two discrete intervals of glaciation separated by a greenhouse interval, and there is no robust evidence for icehouse climate conditions in the terminal Ediacaran immediately preceding the Phanerozoic Eon. We encourage rigorous testing of the climatic and biotic framework we propose here, which from available evidence supports a Phanerozoic-style coupling of metazoan life and climate since the Ediacaran Period.

**ACKNOWLEDGEMENTS**

We gratefully acknowledge funding from The Leverhulme Trust, grant RPG-2022-233 to MW, THPH, AGL and AP (Earth System dynamics at the dawn of the animal-rich biosphere), and the NERC C-CLEAR DTP (supporting the PhD studentship of BHT). We are grateful to Graham Shields for helpful discussions about specific deposits, and to Georgina Virgo and Carol Dehler whose comments greatly improved a previous version of this manuscript.

**REFERENCES CITED**

Agić, H., Jensen, S., Meinhold, G., Högström, A.E.S., Ebbestad, J.O.R., Høyberget, M., Palacios, T., and Taylor, W.L., 2024, Life through an Ediacaran glaciation: Shale- and diamictite-hosted organic-walled microfossil assemblages from the late Neoproterozoic of the Tanafjorden area, northern Norway: Palaeogeography, Palaeoclimatology, Palaeoecology, v. 635, p. 111956, doi:10.1016/j.palaeo.2023.111956.

Alroy, J., 2014, Accurate and precise estimates of origination and extinction rates: Paleobiology, v. 40, p. 374–397, doi:10.1666/13036.

Alroy, J., 2010a, Fair Sampling of Taxonomic Richness and Unbiased Estimation of Origination and Extinction Rates: The Paleontological Society Papers, v. 16, p. 55–80, doi:10.1017/S1089332600001819.

Alroy, J., 2010b, Geographical, environmental and intrinsic biotic controls on Phanerozoic marine diversification: Palaeontology, v. 53, p. 1211–1235, doi:10.1111/j.1475-4983.2010.01011.x.

Álvaro, J.J., Cortijo, I., Jensen, S., Lorenzo, S., and Pieren, A.P., 2019, Updated stratigraphic framework and biota of the Ediacaran and Terreneuvian in the Alcudia-Toledo Mountains of the Central Iberian Zone, Spain: Estudios Geológicos, v. 75, p. e093–e093, doi:10.3989/egeol.43620.548.

Álvaro, J.J., Johnson, S.C., Barr, S.M., Jensen, S., Palacios, T., van Rooyen, D., and White, C.E., 2022, Unconformity-bounded rift sequences in Terreneuvian–Miaolingian strata of the Caledonian Highlands, Atlantic Canada: GSA Bulletin, v. 135, p. 1225–1242, doi:10.1130/B36402.1.

Amorim, K.B., Afonso, J.W.L., Leme, J. de M., Diniz, C.Q.C., Rivera, L.C.M., Gómez-Gutiérrez, J.C., Boggiani, P.C., and Trindade, R.I.F., 2020, Sedimentary facies, fossil distribution and depositional setting of the late Ediacaran Tamengo Formation (Brazil): Sedimentology, v. 67, p. 3422–3450, doi:10.1111/sed.12749.

Arnaud, E., Halverson, G.P., and Shields-Zhou, G., 2011, The Geological Record of Neoproterozoic Glaciations: Geological Society of London, doi:10.1144/M36.

Bergmann, K., Osburn, M.R., Wilcots, J., Cantine, M., Grotzinger, J.P., Fischer, W.W., Eiler, J.M., and Bonifacie, M., 2022, The Shuram excursion: A response to climate extremes at the dawn of animal life:, doi:10.1002/essoar.10511917.1.

Berkman, P.A., Cattaneo-Vietti, R., Chiantore, M., and Howard-Williams, C., 2004, Polar emergence and the influence of increased sea-ice extent on the Cenozoic biogeography of pectinid molluscs in Antarctic coastal areas: Deep Sea Research Part II: Topical Studies in Oceanography, v. 51, p. 1839–1855, doi:10.1016/j.dsr2.2004.07.017.

Berner, R.A., 2006, Inclusion of the Weathering of Volcanic Rocks in the GEOCARBSULF Model: American Journal of Science, v. 306, p. 295–302, doi:10.2475/05.2006.01.

Berner, R.A., 2004, The Phanerozoic Carbon Cycle: CO2 and O2: Oxford University Press, USA, 159 p.

Betts, M.J. et al., 2018, Early Cambrian chronostratigraphy and geochronology of South Australia: Earth-Science Reviews, v. 185, p. 498–543, doi:10.1016/j.earscirev.2018.06.005.

Blein, O. et al., 2014, Geochronological constraints on the polycyclic magmatism in the Bou Azzer-El Graara inlier (Central Anti-Atlas Morocco): Journal of African Earth Sciences, v. 99, p. 287–306, doi:10.1016/j.jafrearsci.2014.04.021.

Boag, T.H., Busch, J.F., Gooley, J.T., Strauss, J.V., and Sperling, E.A., 2024, Deep-water first occurrences of Ediacara biota prior to the Shuram carbon isotope excursion in the Wernecke Mountains, Yukon, Canada: Geobiology, v. 22, p. e12597, doi:10.1111/gbi.12597.

Boag, T.H., Darroch, S.A.F., and Laflamme, M., 2016, Ediacaran distributions in space and time: testing assemblage concepts of earliest macroscopic body fossils: Paleobiology, v. 42, p. 574–594, doi:10.1017/pab.2016.20.

Boag, T.H., Stockey, R.G., Elder, L.E., Hull, P.M., and Sperling, E.A., 2018, Oxygen, temperature and the deep-marine stenothermal cradle of Ediacaran evolution: Proceedings of the Royal Society B: Biological Sciences, v. 285, p. 20181724, doi:10.1098/rspb.2018.1724.

Boddy, C.E., Mitchell, E.G., Merdith, A., and Liu, A.G., 2021, Palaeolatitudinal distribution of the Ediacaran macrobiota: Journal of the Geological Society, doi:10.1144/jgs2021-030.

Bond, D.P.G., and Grasby, S.E., 2017, On the causes of mass extinctions: Palaeogeography, Palaeoclimatology, Palaeoecology, v. 478, p. 3–29, doi:10.1016/j.palaeo.2016.11.005.

Bossi, J., Cingolani, C.A., Llambías, E.J., Varela, R., and Campal, N., 1993, Características del magmatismo post-orogénico finibrasiliano en el Uruguay: formaciones Sierra de Ríos y Sierra de Ánimas: Brazilian Journal of Geology, v. 23, no. 3, doi:10.5327/rbg.v23i3.469.

Boucot, A.J., Xu, C., Scotese, C.R., and Morley, R.J., 2013, Phanerozoic Paleoclimate: An Atlas of Lithologic Indicators of Climate: SEPM (Society for Sedimentary Geology), SEPM Concepts in Sedimentology and Paleontology 11, 478 p.

Bowring, S.A., Grotzinger, J.P., Condon, D.J., Ramezani, J., Newall, M.J., and Allen, P.A., 2007, Geochronologic constraints on the chronostratigraphic framework of the Neoproterozoic Huqf Supergroup, Sultanate of Oman: American Journal of Science, v. 307, p. 1097–1145, doi:10.2475/10.2007.01.

Bowyer, F.T., Uahengo, C.-I., Kaputuaza, K., Ndeunyema, J., Yilales, M., Alexander, R.D., Curtis, A., and Wood, R.A., 2023, Constraining the onset and environmental setting of metazoan biomineralization: The Ediacaran Nama Group of the Tsaus Mountains, Namibia: Earth and Planetary Science Letters, v. 620, p. 118336, doi:10.1016/j.epsl.2023.118336.

Bowyer, F.T., Wood, R.A., and Yilales, M., 2024, Sea level controls on Ediacaran-Cambrian animal radiations: Science Advances, v. 10, p. eado6462, doi:10.1126/sciadv.ado6462.

Bowyer, F.T., Zhuravlev, A.Y., Wood, R., Shields, G.A., Zhou, Y., Curtis, A., Poulton, S.W., Condon, D.J., Yang, C., and Zhu, M., 2022, Calibrating the temporal and spatial dynamics of the Ediacaran - Cambrian radiation of animals: Earth-Science Reviews, v. 225, p. 103913, doi:10.1016/j.earscirev.2021.103913.

Busch, J.F., Boag, T.H., Sperling, E.A., Rooney, A.D., Feng, X., Moynihan, D.P., and Strauss, J.V., 2023, Integrated Litho-, Chemo- and Sequence Stratigraphy of the Ediacaran Gametrail Formation Across a Shelf-Slope Transect in the Wernecke Mountains, Yukon, Canada: American Journal of Science, v. 323, p. 4, doi:10.2475/001c.74874.

Busch, J.F., Hodgin, E.B., Ahm, A.-S.C., Husson, J.M., Macdonald, F.A., Bergmann, K.D., Higgins, J.A., and Strauss, J.V., 2022, Global and local drivers of the Ediacaran Shuram carbon isotope excursion: Earth and Planetary Science Letters, v. 579, p. 117368, doi:10.1016/j.epsl.2022.117368.

Butterfield, N.J., 2009, Macroevolutionary turnover through the Ediacaran transition: ecological and biogeochemical implications: Geological Society, London, Special Publications, v. 326, p. 55–66, doi:10.1144/SP326.3.

Cantine, M.D., Rooney, A.D., Knoll, A.H., Gómez-Pérez, I., al Baloushi, B., and Bergmann, K.D., 2024, Chronology of Ediacaran sedimentary and biogeochemical shifts along eastern Gondwanan margins: Communications Earth & Environment, v. 5, p. 1–9, doi:10.1038/s43247-024-01630-1.

Carbone, C.A., Narbonne, G.M., Macdonald, F.A., and Boag, T.H., 2015, New Ediacaran fossils from the uppermost Blueflower Formation, northwest Canada: disentangling biostratigraphy and paleoecology: Journal of Paleontology, v. 89, p. 281–291, doi:10.1017/jpa.2014.25.

Carto, S.L., and Eyles, N., 2011, Chapter 42 The deep-marine glaciogenic Gaskiers Formation, Newfoundland, Canada: Geological Society, London, Memoirs, v. 36, p. 467–473, doi:10.1144/M36.42.

Carto, S.L., and Eyles, N., 2012, Sedimentology of the Neoproterozoic (c. 580 Ma) Squantum ‘Tillite’, Boston Basin, USA: Mass flow deposition in a deep-water arc basin lacking direct glacial influence: Sedimentary Geology, v. 269–270, p. 1–14, doi:10.1016/j.sedgeo.2012.03.011.

Chumakov, N.M., 2011, Chapter 24 The Neoproterozoic glacial formations of the North and Middle Urals, *in* Arnaud, E., Halverson, G.P., and Shields-Zhou, G. eds., The Geological

Record of Neoproterozoic Glaciations, Geological Society of London, Geological Society, London, Memoirs 36, p. 289–296, doi:10.1144/M36.23.

Chumakov, N.M., 2009, The Baykonurian glaciohorizon of the Late Vendian: Stratigraphy and Geological Correlation, v. 17, p. 373–381, doi:10.1134/S0869593809040029.

Chumakov, N.M., Pokrovskii, B.G., and Maslov, A.V., 2013, Stratigraphic position and significance of carbonate rocks related to neoproterozoic glacial horizons of the Urals: Stratigraphy and Geological Correlation, v. 21, p. 573–591, doi:10.1134/S0869593813060038.

Clarke, A., and Crame, J.A., 1992, The Southern Ocean benthic fauna and climate change: a historical perspective: Philosophical Transactions of the Royal Society of London. Series B: Biological Sciences, v. 338, p. 299–309, doi:10.1098/rstb.1992.0150.

Clarke, A.J.I., Kirkland, C.L., Menon, L.R., Condon, D.J., Cope, J.C.W., Bevins, R.E., and Glorie, S., 2024, U–Pb zircon–rutile dating of the Llangynog Inlier, Wales: constraints on an Ediacaran shallow-marine fossil assemblage from East Avalonia: Journal of the Geological Society, v. 181, p. jgs2023- 081, doi:10.1144/jgs2023-081.

Cohen, K.M., Finney, S.C., Gibbard, P.L., and Fan, J.-X., 2013, The ICS International Chronostratigraphic Chart v 2023/09: Episodes, v. 36, p. 199–204, doi:10.18814/epiiugs/2013/v36i3/002.

Cope, J.C.W., 1977, An Ediacara-type fauna from South Wales: Nature, v. 268, p. 624–624, doi:10.1038/268624a0.

Cope, J.C.W., 1983, Precambrian faunas from the Carmarthen district: Nature in Wales, v. 1, p. 11–16.

Darroch, S.A.F. et al., 2015, Biotic replacement and mass extinction of the Ediacara biota: Proceedings of the Royal Society B: Biological Sciences, v. 282, p. 20151003, doi:10.1098/rspb.2015.1003.

Deutsch, C., Ferrel, A., Seibel, B., Pörtner, H.-O., and Huey, R.B., 2015, Climate change tightens a metabolic constraint on marine habitats: Science, v. 348, p. 1132–1135, doi:10.1126/science.aaa1605.

Dott, R.H., Jr., 1961, Squantum "Tillite", Massachusetts—Evidence of Glaciation or Subaqueous Mass Movements? GSA Bulletin, v. 72, p. 1289–1305, doi:10.1130/0016-7606(1961)72[1289:STMOGO]2.0.CO;2.

Dunn, F.S., Kenchington, C.G., Parry, L.A., Clark, J.W., Kendall, R.S., and Wilby, P.R., 2022, A crown-group cnidarian from the Ediacaran of Charnwood Forest, UK: Nature Ecology & Evolution, v. 6, p. 1095–1104, doi:10.1038/s41559-022-01807-x.

Erwin, D.H., 2009, Climate as a Driver of Evolutionary Change: Current Biology, v. 19, p. R575–R583, doi:10.1016/j.cub.2009.05.047.

Etemad-Saeed, N., Hosseini-Barzi, M., Adabi, M.H., Miller, N.R., Sadeghi, A., Houshmandzadeh, A., and Stockli, D.F., 2016, Evidence for ca. 560 Ma Ediacaran glaciation in the Kahar Formation, central Alborz Mountains, northern Iran: Gondwana Research, v. 31, p. 164–183, doi:10.1016/j.gr.2015.01.005.

Evans, S.D., Diamond, C.W., Droser, M.L., and Lyons, T.W., 2018, Dynamic oxygen and coupled biological and ecological innovation during the second wave of the Ediacara Biota (T. W. Lyons, M. L. Droser, K. V. Lau, & S. M. Porter, Eds.): Emerging Topics in Life Sciences, v. 2, p. 223–233, doi:10.1042/ETLS20170148.

Evans, S.D., Tu, C., Rizzo, A., Surprenant, R.L., Boan, P.C., McCandless, H., Marshall, N., Xiao, S., and Droser, M.L., 2022, Environmental drivers of the first major animal extinction across the Ediacaran White Sea-Nama transition: Proceedings of the National Academy of Sciences, v. 119, p. e2207475119, doi:10.1073/pnas.2207475119.

Fedonkin, M.A., Vickers-Rich, P., Swalla, B.J., Trusler, P., and Hall, M., 2012, A new metazoan from the Vendian of the White Sea, Russia, with possible affinities to the ascidians: Paleontological Journal, v. 46, p. 1–11, doi:10.1134/S0031030112010042.

Fenton, I.S., Aze, T., Farnsworth, A., Valdes, P., and Saupe, E.E., 2023, Origination of the modern-style diversity gradient 15 million years ago: Nature, p. 1–5, doi:10.1038/s41586-023-05712-6.

Fitzgerald, D.M., Narbonne, G.M., Pufahl, P.K., and Dalrymple, R.W., 2024, The Mall Bay Formation (Ediacaran) and the protracted onset of the Gaskiers glaciation in Newfoundland, Canada: Precambrian Research, v. 405, p. 107369, doi:10.1016/j.precamres.2024.107369.

Gaucher, C., Blanco, G., Chiglino, L., Poiré, D., and Germs, G.J.B., 2008, Acritarchs of Las Ventanas Formation (Ediacaran, Uruguay): Implications for the timing of coeval rifting and glacial events in western Gondwana: Gondwana Research, v. 13, p. 488–501, doi:10.1016/j.gr.2007.05.008.

Gehling, J.G., and Droser, M.L., 2013, How well do fossil assemblages of the Ediacara Biota tell time? Geology, v. 41, p. 447–450, doi:10.1130/G33881.1.

Gehling, J.G., and Narbonne, G.M., 2007, Spindle-shaped Ediacara fossils from the Mistaken Point assemblage, Avalon Zone, Newfoundland: Canadian Journal of Earth Sciences, v. 44, p. 367–387, doi:10.1139/e07-003.

Gehling, J.G., Narbonne, G.M., and Anderson, M.M., 2000, The first named Ediacaran body fossil, *Aspidella terranovica*: Palaeontology, v. 43, p. 427–456, doi:10.1111/j.0031-0239.2000.00134.x.

Germs, G.J.B., and Gaucher, C., 2012, Nature and extent of a late Ediacaran (ca. 547 Ma) glacigenic erosion surface in southern Africa: South African Journal of Geology, v. 115, p. 91–102, doi:10.2113/gssajg.115.91.

Grazhdankin, D., 2004, Patterns of distribution in the Ediacaran biotas: facies versus biogeography and evolution: Paleobiology, v. 30, p. 203–221, doi:10.1666/0094-8373(2004)030<0203:PODITE>2.0.CO;2.

Grazhdankin, D., 2014, Patterns of Evolution of the Ediacaran Soft-Bodied Biota: Journal of Paleontology, v. 88, p. 269–283, doi:10.1666/13-072.

Grazhdankin, D.V., Marusin, V.V., Meert, J., Krupenin, M.T., and Maslov, A.V., 2011, Kotlin regional stage in the South Urals: Doklady Earth Sciences, v. 440, p. 1222–1226, doi:10.1134/S1028334X11090170.

Grazhdankin, D.V., Maslov, A.V., and Krupenin, M.T., 2009, Structure and depositional history of the Vendian Sylvitsa Group in the western flank of the Central Urals: Stratigraphy and Geological Correlation, v. 17, p. 476–492, doi:10.1134/S0869593809050025.

Griffiths, H.J., Whittle, R.J., and Mitchell, E.G., 2023, Animal survival strategies in Neoproterozoic ice worlds: Global Change Biology, v. 29, p. 10–20, doi:10.1111/gcb.16393.

Hallam, A., and Wignall, P.B., 1999, Mass extinctions and sea-level changes: Earth-Science Reviews, v. 48, p. 217–250, doi:10.1016/S0012-8252(99)00055-0.

Halverson, G.P., Hoffman, P.F., Schrag, D.P., Maloof, A.C., and Rice, A.H.N., 2005, Toward a Neoproterozoic composite carbon-isotope record: GSA Bulletin, v. 117, p. 1181–1207, doi:10.1130/B25630.1.

Hambrey, M.J., and Harland, W.B., 1981, Criteria for the identification of glacigenic deposits, *in* Hambrey, M.J. and Harland, W.B. eds., Earth's pre-pleistocene glacial record, Cambridge, UK, Cambridge University Press, p. 14–21, https://unesdoc.unesco.org/ark:/48223/pf0000141486 (accessed March 2024).

Hawco, J.B., Kenchington, C.G., and McIlroy, D., 2021, A quantitative and statistical discrimination of morphotaxa within the Ediacaran genus Palaeopascichnus: Papers in Palaeontology, v. 7, p. 657–673, doi:10.1002/spp2.1290.

Hoffman, P.F. et al., 2017, Snowball Earth climate dynamics and Cryogenian geology-geobiology: Science Advances, v. 3, p. e1600983, doi:10.1126/sciadv.1600983.

Hofmann, H.J., Fritz, W.H., and Narbonne, G.M., 1983, Ediacaran (Precambrian) Fossils from the Wernecke Mountains, Northwestern Canada: Science, v. 221, p. 455–457, doi:10.1126/science.221.4609.455.

Hofmann, H.J., O'Brien, S.J., and King, A.F., 2008, Ediacaran Biota on Bonavista Peninsula, Newfoundland, Canada: Journal of Paleontology, v. 82, p. 1–36.

Högström, A., Jensen, S., Palacios, T., and Ebbestad, J.O.R., 2013, New information on the Ediacaran-Cambrian transition in the Vestertana Group, Finnmark, northern Norway, from trace fossils and organic-walled microfossils: Norsk Geologisk Tidsskrift, v. 93, p. 95–106.

Hu, W., and McSaveney, M.J., 2018, A polished and striated pavement formed by a rock avalanche in under 90 s mimics a glacially striated pavement: Geomorphology, v. 320, p. 154–161, doi:10.1016/j.geomorph.2018.08.011.

Inglis, J.D., MacLean, J.S., Samson, S.D., D'Lemos, R.S., Admou, H., and Hefferan, K., 2004, A precise U–Pb zircon age for the Bleïda granodiorite, Anti-Atlas, Morocco: implications for the timing of deformation and terrane assembly in the eastern Anti-Atlas: Journal of African Earth Sciences, v. 39, p. 277–283, doi:10.1016/j.jafrearsci.2004.07.041.

Jensen, S., Högström, A.E.S., Høyberget, M., Meinhold, G., McIlroy, D., Ebbestad, J.O.R., Taylor, W.L., Agić, H., and Palacios, T., 2018, New occurrences of Palaeopascichnus from the Stáhpogieddi Formation, Arctic Norway, and their bearing on the age of the

Varanger Ice Age: Canadian Journal of Earth Sciences, v. 55, p. 1253–1261, doi:10.1139/cjes-2018-0035.

Johnson, S., McLeod, M., and Branscombe, L., 2019, A note on the location of diamictite in the Ratcliffe Brook Group on Hanford Brook, southern New Brunswick, Canada, *in* The Atlantic Geoscience Society (AGS) La Société Géoscientifique de l'Atlantique, p. 35–36, http://ags.earthsciences.dal.ca/Colloquium/program_and_abstracts_2019.pdf.

Keller, C.B., Husson, J.M., Mitchell, R.N., Bottke, W.F., Gernon, T.M., Boehnke, P., Bell, E.A., Swanson-Hysell, N.L., and Peters, S.E., 2019, Neoproterozoic glacial origin of the Great Unconformity: Proceedings of the National Academy of Sciences, v. 116, p. 1136–1145, doi:10.1073/pnas.1804350116.

Kenchington, C.G., Harris, S.J., Vixseboxse, P.B., Pickup, C., and Wilby, P.R., 2018, The Ediacaran fossils of Charnwood Forest: Shining new light on a major biological revolution: Proceedings of the Geologists' Association, v. 129, p. 264–277, doi:10.1016/j.pgeola.2018.02.006.

Kennedy, K., and Eyles, N., 2021, Syn-rift mass flow generated 'tectonofacies' and 'tectonosequences' of the Kingston Peak Formation, Death Valley, California, and their bearing on supposed Neoproterozoic panglacial climates: Sedimentology, v. 68, p. 352–381, doi:10.1111/sed.12781.

Kennedy, K., Eyles, N., and Broughton, D., 2019, Basinal setting and origin of thick (1·8 km) mass-flow dominated Grand Conglomérat diamictites, Kamoa, Democratic Republic of

Congo: Resolving climate and tectonic controls during Neoproterozoic glaciations: Sedimentology, v. 66, p. 556–589, doi:10.1111/sed.12494.

Kocsis, Á.T., Reddin, C.J., Alroy, J., and Kiessling, W., 2019, The r package divDyn for quantifying diversity dynamics using fossil sampling data: Methods in Ecology and Evolution, v. 10, p. 735–743, doi:10.1111/2041-210X.13161.

Kröner, A., 1981, A29. Late Precambrian diamictites of South Africa and Namibia, *in* Hambrey, M.J. and Harland, W.B. eds., Earth's pre-pleistocene glacial record, Cambridge, UK, Cambridge University Press, p. 167–177, https://unesdoc.unesco.org/ark:/48223/pf0000141486 (accessed March 2024).

Kröner, A., and Germs, G.J.B., 1971, A re-interpretation of the Numees-Nama contact at Aussenkjer, southwest Africa: Transactions of the Geological Soceity of South Africa, v. 74, p. 69–74.

Kühnemann, V., Meinhold, G., Schulz, B., Gilbricht, S., Weber, S., and Wemmer, K., 2024, The "greywacke problem" explored in the neoproterozoic of Saxo-Thuringia: new insights into sediment composition and metamorphic overprint: International Journal of Earth Sciences, doi:10.1007/s00531-024-02475-x.

Le Heron, D.P., Vandyk, T.M., Kuang, H., Liu, Y., Chen, X., Wang, Y., Yang, Z., Scharfenberg, L., Davies, B., and Shields, G., 2019, Bird's-eye view of an Ediacaran subglacial landscape: Geology, v. 47, p. 705–709, doi:10.1130/G46285.1.

Letsch, D., Large, S.J.E., Buechi, M.W., Winkler, W., and von Quadt, A., 2018, Ediacaran glaciations of the west African Craton – Evidence from Morocco: Precambrian Research, v. 310, p. 17–38, doi:10.1016/j.precamres.2018.02.015.

Linnemann, U. et al., 2018, A ~565 Ma old glaciation in the Ediacaran of peri-Gondwanan West Africa: International Journal of Earth Sciences, v. 107, p. 885–911, doi:10.1007/s00531-017-1520-7.

Linnemann, U. et al., 2022, An Upper Ediacaran Glacial Period in Cadomia: the Granville tillite (Armorican Massif) – sedimentology, geochronology and provenance: Geological Magazine, v. 159, p. 999–1013, doi:10.1017/S0016756821001011.

Linnemann, U. et al., 2019, New high-resolution age data from the Ediacaran–Cambrian boundary indicate rapid, ecologically driven onset of the Cambrian explosion: Terra Nova, v. 31, p. 49–58, doi:10.1111/ter.12368.

Liu, A.G., 2011, Reviewing the Ediacaran fossils of the Long Mynd, Shropshire: Proceedings of the Shropshire Geological Society, v. 16, p. 31–43.

Liu, A.G., Kenchington, C.G., and Mitchell, E.G., 2015, Remarkable insights into the paleoecology of the Avalonian Ediacaran macrobiota: Gondwana Research, v. 27, p. 1355–1380, doi:10.1016/j.gr.2014.11.002.

Liu, A.G., Matthews, J.J., Menon, L.R., McIlroy, D., and Brasier, M.D., 2014a, *Haootia quadriformis* n. gen., n. sp., interpreted as a muscular cnidarian impression from the Late Ediacaran period (approx. 560 Ma): Proceedings of the Royal Society B: Biological Sciences, v. 281, p. 20141202–20141202, doi:10.1098/rspb.2014.1202.

Liu, A.G., McIlroy, D., Matthews, J.J., and Brasier, M.D., 2014b, Confirming the metazoan character of a 565 Ma trace-fossil assemblage from Mistaken Point, Newfoundland: PALAIOS, v. 29, p. 420–430, doi:10.2110/palo.2014.011.

Liu, A.G., Mcllroy, D., and Brasier, M.D., 2010, First evidence for locomotion in the Ediacara biota from the 565 Ma Mistaken Point Formation, Newfoundland: Geology, v. 38, p. 123–126, doi:10.1130/G30368.1.

Macdonald, F.A., Swanson-Hysell, N.L., Park, Y., Lisiecki, L., and Jagoutz, O., 2019, Arc-continent collisions in the tropics set Earth's climate state: Science, v. 364, p. 181–184, doi:10.1126/science.aav5300.

Mallmann, G., Chemale, F., Ávila, J.N., Kawashita, K., and Armstrong, R.A., 2007, Isotope geochemistry and geochronology of the Nico Pérez Terrane, Rio de la Plata Craton, Uruguay: Gondwana Research, v. 12, p. 489–508, doi:10.1016/j.gr.2007.01.002.

Martin, H., 1965, The Precambrian geology of south West Africa and Namaqualand: Cape Town, University of Cape Town, Precambrian, p. 4 pl.

Martin, M.W., Grazhdankin, D.V., Bowring, S.A., Evans, D.A.D., Fedonkin, M.A., and Kirschvink, J.L., 2000, Age of Neoproterozoic Bilaterian Body and Trace Fossils, White Sea, Russia: Implications for Metazoan Evolution: Science, v. 288, p. 841–845.

Maslov, A., Meert, J., Levashova, N., Yu, R., Grazhdankin, D., Kuznetsov, N., Krupenin, M., Fedorova, N.M., and Ipat`eva, I.S., 2013, New Constraints for the Age of Vendian Glacial Deposits (Central Urals): Doklady Earth Sciences, v. 449, p. 303–308, doi:10.1134/S1028334X13030203.

Matthews, J.J., 2015, The stratigraphical context of the Ediacaran Biota of eastern Newfoundland: University of Oxford, https://ora.ox.ac.uk/objects/uuid:852682cc-aa5a-42b9-83fd-4dd013ebc21b (accessed May 2018).

Matthews, J.J., Liu, A.G., Yang, C., McIlroy, D., Levell, B., and Condon, D.J., 2020, A Chronostratigraphic Framework for the Rise of the Ediacaran Macrobiota: New Constraints from Mistaken Point Ecological Reserve, Newfoundland: GSA Bulletin, v. 133, p. 612–624, doi:10.1130/B35646.1.

McIlroy, D., and Brasier, M.D., 2017, Ichnological evidence for the Cambrian explosion in the Ediacaran to Cambrian succession of Tanafjord, Finnmark, northern Norway: Geological Society, London, Special Publications, v. 448, p. 351–368, doi:10.1144/SP448.7.

McMahon, W.J., Liu, A.G., Tindal, B.H., and Kleinhans, M.G., 2020, Ediacaran life close to land: Coastal and shoreface habitats of the Ediacaran macrobiota, the Central Flinders Ranges, South Australia: Journal of Sedimentary Research, v. 90, p. 1463–1499, doi:10.2110/jsr.2020.029.

Meinhold, G., Arslan, A., Jensen, S., and Kühnemann, V., 2025, Discovery of trace fossils in the Weesenstein Group, Elbe Zone, Germany, and its significance for revising the Ediacaran and Ordovician stratigraphy of Saxo-Thuringia: Geological Magazine, v. 162, p. e10, doi:10.1017/S0016756825000032.

Menon, L., 2015, Ediacaran discoidal impressions and related structures from Newfoundland, Canada and the Long Mynd, Shropshire, UK: their nature and biogenicity [http://purl.org/dc/dcmitype/Text]: University of Oxford, https://ora.ox.ac.uk/objects/uuid:ff1dc37f-711d-41f2-a3b8-733cd26cb571 (accessed August 2024).

Menon, L.R., McIlroy, D., and Brasier, M.D., 2013, Evidence for Cnidaria-like behavior in ca. 560 Ma Ediacaran Aspidella: Geology, v. 41, p. 895–898, doi:10.1130/G34424.1.

Miller, N., Johnson, P., and Stern, B., 2008, Marine versus non-marine environments for the Jibalah Group, NW Arabian shield: A sedimentologic and geochemical survey and report of possible metazoa in the Dhaiqa formation: Arabian Journal for Science and Engineering, v. 33, p. 55–77.

Mills, B.J.W., Krause, A.J., Scotese, C.R., Hill, D.J., Shields, G.A., and Lenton, T.M., 2019, Modelling the long-term carbon cycle, atmospheric CO2, and Earth surface temperature from late Neoproterozoic to present day: Gondwana Research, v. 67, p. 172–186, doi:10.1016/j.gr.2018.12.001.

Mills, A.J., Normore, L., Gomez, N., Dunning, G.R., and Lowe, D.G., 2024, A tale of two basins: juxtaposition of the Ediacaran fossil-bearing St. John’s Basin against the Ediacaran glaciovolcanic Bonavista Basin on the Bonavista Peninsula, Avalon Zone, Newfoundland: Atlantic Geoscience, v. 60, p. 131–150, doi:10.4138/atlgeo.2024.007.

Molén, M.O., 2023, Glaciation-induced features or sediment gravity flows – An analytic review: Journal of Palaeogeography, v. 12, p. 487–545, doi:10.1016/j.jop.2023.08.002.

Moynihan, D.P., Strauss, J.V., Nelson, L.L., and Padget, C.D., 2019, Upper Windermere Supergroup and the transition from rifting to continent-margin sedimentation, Nadaleen

River area, northern Canadian Cordillera: GSA Bulletin, v. 131, p. 1673–1701, doi:10.1130/B32039.1.

Muscente, A.D. et al., 2019, Ediacaran biozones identified with network analysis provide evidence for pulsed extinctions of early complex life: Nature Communications, v. 10, p. 911, doi:10.1038/s41467-019-08837-3.

Narbonne, G.M., 2005, The Ediacara Biota: Neoproterozoic Origin of Animals and Their Ecosystems: Annual Review of Earth and Planetary Sciences, v. 33, p. 421–442, doi:10.1146/annurev.earth.33.092203.122519.

Narbonne, G.M., and Hofmann, H.J., 1987, Ediacaran biota of the Wernecke Mountains, Yukon, Canada: Palaeontology, v. 30, p. 647–676.

Narbonne, G.M., Laflamme, M., Trusler, P.W., Dalrymple, R.W., and Greentree, C., 2014, Deep-Water Ediacaran Fossils from Northwestern Canada: Taphonomy, Ecology, and Evolution: Journal of Paleontology, v. 88, p. 207–223, doi:10.1666/13-053.

Nelson, L.L., Ramezani, J., Almond, J.E., Darroch, S.A.F., Taylor, W.L., Brenner, D.C., Furey, R.P., Turner, M., and Smith, E.F., 2022, Pushing the boundary: A calibrated Ediacaran-Cambrian stratigraphic record from the Nama Group in northwestern Republic of South Africa: Earth and Planetary Science Letters, v. 580, p. 117396, doi:10.1016/j.epsl.2022.117396.

Niu, Y., Shi, G.R., Zhang, Q., Jones, B.G., Wang, X., and Zhao, G., 2024, Ediacaran Cordilleran-type mountain ice sheets and their erosion effects: Earth-Science Reviews, v. 249, p. 104671, doi:10.1016/j.earscirev.2023.104671.

Noble, S.R., Condon, D.J., Carney, J.N., Wilby, P.R., Pharaoh, T.C., and Ford, T.D., 2015, U-Pb geochronology and global context of the Charnian Supergroup, UK: Constraints on the age of key Ediacaran fossil assemblages: GSA Bulletin, v. 127, p. 250–265, doi:10.1130/B31013.1.

O'Connell, B., McMahon, W.J., Nduutepo, A., Pokolo, P., Mocke, H., McMahon, S., Boddy, C.E., and Liu, A.G., 2024, Transport of 'Nama'-type biota in sediment gravity and combined flows: Implications for terminal Ediacaran palaeoecology: Sedimentology, doi:10.1111/sed.13239.

Oyhantçabal, P., Siegesmund, S., Wemmer, K., Frei, R., and Layer, P., 2007, Post-collisional transition from calc-alkaline to alkaline magmatism during transcurrent deformation in the southernmost Dom Feliciano Belt (Braziliano–Pan-African, Uruguay): Lithos, v. 98, p. 141–159, doi:10.1016/j.lithos.2007.03.001.

Palacios, T., 2024, The oldest fossil record in the Iberian Peninsula; lower Ediacaran acritarchs of the Tentudía Formation, Ossa-Morena Zone (OMZ), Southwest Iberian Massif.: Journal of Iberian Geology, doi:10.1007/s41513-024-00266-6.

Pang, K., Wu, C., Sun, Y., Ouyang, Q., Yuan, X., Shen, B., Lang, X., Wang, R., Chen, Z., and Zhou, C., 2021, New Ediacara-type fossils and late Ediacaran stratigraphy from the northern Qaidam Basin (China): Paleogeographic implications: Geology, v. 49, p. 1160–1164, doi:10.1130/G48842.1.

Pauley, J.C., 1991, A revision of the stratigraphy of the longmyndian supergroup, welsh borderland, and of its relationship to the uriconian volcanic complex: Geological Journal, v. 26, p. 167–183, doi:10.1002/gj.3350260209.

Pazos, P.J., Rapalini, A.E., Bettucci, L.S., and Tófalo, O.R., 2011, Chapter 52 The Playa Hermosa Formation, Playa Verde Basin, Uruguay: Geological Society, London, Memoirs, v. 36, p. 547–553, doi:10.1144/M36.52.

Pecoits, E., 2003, Sedimentología y consideraciones estratigráficas de la Formación Las Ventanas en su área tipo, Departamento de Maldonado, Uruguay: Revista de la Sociedad Uruguaya de Geologia Publicacion Especial, v. 1, p. 124–140.

Pecoits, E., Gingras, M., Aubet, N., and Konhauser, K., 2008, Ediacaran in Uruguay: palaeoclimatic and palaeobiological implications: Sedimentology, v. 55, p. 689–719, doi:10.1111/j.1365-3091.2007.00918.x.

Pecoits, E., Gingras, M.K., and Konhauser, K.O., 2011, Chapter 53 Las Ventanas and San Carlos formations, Maldonado Group, Uruguay: Geological Society, London, Memoirs, v. 36, p. 555–564, doi:10.1144/M36.53.

Penn, J.L., Deutsch, C., Payne, J.L., and Sperling, E.A., 2018, Temperature-dependent hypoxia explains biogeography and severity of end-Permian marine mass extinction: Science, v. 362, doi:10.1126/science.aat1327.

Perry, A.L., Low, P.J., Ellis, J.R., and Reynolds, J.D., 2005, Climate Change and Distribution Shifts in Marine Fishes: Science, v. 308, p. 1912–1915, doi:10.1126/science.1111322.

Peters, S.E., and Gaines, R.R., 2012, Formation of the ‘Great Unconformity’ as a trigger for the Cambrian explosion: Nature, v. 484, p. 363–366, doi:10.1038/nature10969.

Pu, J.P., Bowring, S.A., Ramezani, J., Myrow, P., Raub, T.D., Landing, E., Mills, A., Hodgin, E., and Macdonald, F.A., 2016, Dodging snowballs: Geochronology of the Gaskiers glaciation and the first appearance of the Ediacaran biota: Geology, v. 44, p. 955–958, doi:10.1130/G38284.1.

Pyle, L.J., Narbonne, G.M., James, N.P., Dalrymple, R.W., and Kaufman, A.J., 2004, Integrated Ediacaran chronostratigraphy, Wernecke Mountains, northwestern Canada: Precambrian Research, v. 132, p. 1–27, doi:10.1016/j.precamres.2004.01.004.

R Core Team, 2021, R: A Languange and Environment for Statistical Computing:, https://www.R-project.org (accessed January 2025).

Rapalini, A.E., Tohver, E., Bettucci, L.S., Lossada, A.C., Barcelona, H., and Pérez, C., 2015, The late Neoproterozoic Sierra de las Ánimas Magmatic Complex and Playa Hermosa Formation, southern Uruguay, revisited: Paleogeographic implications of new paleomagnetic and precise geochronologic data: Precambrian Research, v. 259, p. 143–155, doi:10.1016/j.precamres.2014.11.021.

Retallack, G.J., 2022, Towards a glacial subdivision of the Ediacaran Period, with an example of the Boston Bay Group, Massachusetts: Australian Journal of Earth Sciences, v. 69, p. 223–250, doi:10.1080/08120099.2021.1954088.

Rice, A.H.N., Edwards, M.B., Hansen, T.A., Arnaud, E., and Halverson, G.P., 2011, Chapter 57 Glaciogenic rocks of the Neoproterozoic Smalfjord and Mortensnes formations, Vestertana Group, E. Finnmark, Norway: Geological Society, London, Memoirs, v. 36, p. 593–602, doi:10.1144/M36.57.

Rooney, A.D., Cantine, M.D., Bergmann, K.D., Gómez-Pérez, I., Baloushi, B.A., Boag, T.H., Busch, J.F., Sperling, E.A., and Strauss, J.V., 2020, Calibrating the coevolution of Ediacaran life and environment: Proceedings of the National Academy of Sciences, doi:10.1073/pnas.2002918117.

Runnegar, B., Gehling, J.G., Jensen, S., and Saltzman, M.R., 2024, Ediacaran paleobiology and biostratigraphy of the Nama Group, Namibia, with emphasis on the erniettomorphs, tubular and trace fossils, and a new sponge, Arimasia germsi n. gen. n. sp.: Journal of Paleontology, v. 98, p. 1–59, doi:10.1017/jpa.2023.81.

Sanchez Bettucci, L., and Linares, E., 1996, Primeras edades en Basaltos del Complejo Sierra de las Animas: XIII Congreso Geológico Argentino y III Congreso de Exploración de Hidrocarburos, Actas, v. 1, p. 399–404.

Schwellnus, C., 1941, The Nama tillite in the Klein Karas Mountains: Transactions Geologic Society of South Africa, v. 44, p. 19–33.

Scotese, C.R., Song, H., Mills, B.J.W., and van der Meer, D.G., 2021, Phanerozoic paleotemperatures: The earth’s changing climate during the last 540 million years: Earth-Science Reviews, v. 215, p. 103503, doi:10.1016/j.earscirev.2021.103503.

Segessenman, D.C., and Peters, S.E., 2024, Transgression–regression cycles drive correlations in Ediacaran–Cambrian rock and fossil records: Paleobiology, v. 50, p. 150–163, doi:10.1017/pab.2023.31.

Shen, B., Xiao, S., Dong, L., Chuanming, Z., and Liu, J., 2007, Problematic macrofossils from Ediacaran successions in the North China and Chaidam blocks: implications for their evolutionary roots and biostratigraphic significance: Journal of Paleontology, v. 81, p. 1396–1411, doi:10.1666/06-016R.1.

Shen, B., Xiao, S., Zhou, C., Kaufman, A.J., and Yuan, X., 2010, Carbon and sulfur isotope chemostratigraphy of the Neoproterozoic Quanji Group of the Chaidam Basin, NW China: Basin stratification in the aftermath of an Ediacaran glaciation postdating the Shuram event? Precambrian Research, v. 177, p. 241–252, doi:10.1016/j.precamres.2009.12.006.

Shields, G.A., Mills, B.J.W., Zhu, M., Raub, T.D., Daines, S.J., and Lenton, T.M., 2019, Unique Neoproterozoic carbon isotope excursions sustained by coupled evaporite dissolution and pyrite burial: Nature Geoscience, p. 1–5, doi:10.1038/s41561-019-0434-3.

Socci, A.D., and Smith, G.W., 1990, Stratigraphic implications of facies within the Boston Basin, *in* Socci, A.D., Skehan, J.W., and Smith, G.W. eds., Geology of the Composite Avalon Terrane of Southern New England, Geological Society of America, v. 245, p. 0, doi:10.1130/SPE245-p55.

Song, H., Huang, S., Jia, E., Dai, X., Wignall, P.B., and Dunhill, A.M., 2020, Flat latitudinal diversity gradient caused by the Permian–Triassic mass extinction: Proceedings of the National Academy of Sciences, v. 117, p. 17578–17583, doi:10.1073/pnas.1918953117.

Stockey, R.G., Pohl, A., Ridgwell, A., Finnegan, S., and Sperling, E.A., 2021, Decreasing Phanerozoic extinction intensity as a consequence of Earth surface oxygenation and metazoan ecophysiology: Proceedings of the National Academy of Sciences, v. 118, doi:10.1073/pnas.2101900118.

Surprenant, R.L., and Droser, M.L., 2024, New insight into the global record of the Ediacaran tubular morphotype: a common solution to early multicellularity: Royal Society Open Science, v. 11, p. 231313, doi:10.1098/rsos.231313.

Tasistro-Hart, A.R., and Macdonald, F.A., 2023, Phanerozoic flooding of North America and the Great Unconformity: Proceedings of the National Academy of Sciences, v. 120, p. e2309084120, doi:10.1073/pnas.2309084120.

Thomas, R.J. et al., 2002, Precambrian evolution of the Sirwa Window, Anti-Atlas Orogen, Morocco: Precambrian Research, v. 118, p. 1–57, doi:10.1016/S0301-9268(02)00075-X.

Thompson, M.D., and Bowring, S.A., 2000, Age of the Squantum "tillite," Boston Basin, Massachusetts; U-Pb zircon constraints on terminal Neoproterozoic glaciation: American Journal of Science, v. 300, p. 630–655, doi:10.2475/ajs.300.8.630.

Thompson, M.D., Grunow, A.M., and Ramezani, J., 2007, Late Neoproterozoic paleogeography of the Southeastern New England Avalon Zone: Insights from U-Pb geochronology and paleomagnetism: GSA Bulletin, v. 119, p. 681–696, doi:10.1130/B26014.1.

Tindal, B., 2023, Geological constraints on Neoproterozoic glacial episodes [PhD]: University of Cambridge, 275 p., https://www.repository.cam.ac.uk/handle/1810/346128 (accessed October 2023).

Vickers-Rich, P. et al., 2013, Reconnaissance for an Ediacaran fauna, Kingdom of Saudi Arabia: Saudi Geological Survey Technical Report SGS-TR-2013-5, 42 p., https://www.researchgate.net/publication/274730804_IN_SEARCH_OF_THE_KINGDOM'S_EDIACARANS_THE_FIRST_GENUINE_METAZOANS_MACROSCOPIC_BODY_AND_TRACE_FOSSILS_FROM_THE_NEOPROTEROZOIC_JIBALAH_GROUP_VENDIANEDIACARAN_ON_THE_ARABIAN_SHIELD (accessed June 2023).

Waggoner, B., 2003, The Ediacaran Biotas in Space and Time: Integrative and Comparative Biology, v. 43, p. 104–113, doi:10.1093/icb/43.1.104.

Wang, X.-P., Chen, Z., Pang, K., Zhou, C.-M., Xiao, S., Wan, B., and Yuan, X.-L., 2021a, *Dickinsonia* from the Ediacaran Dengying Formation in the Yangtze Gorges area, South China: Palaeoworld, v. 30, p. 602–609, doi:10.1016/j.palwor.2021.01.002.

Wang, Z., Chen, C., Wang, J., Suess, E., Chen, X., Ma, X., Wang, G., and Xiao, S., 2020, Wide but not ubiquitous distribution of glendonite in the Doushantuo Formation, South China: Implications for Ediacaran climate: Precambrian Research, v. 338, p. 105586, doi:10.1016/j.precamres.2019.105586.

Wang, C., Evans, D.A.D., Li, M., Zhang, J.-H., Han, J., Wen, B., Wang, J., and Zhao, J.-F., 2022, Proterozoic-Mesozoic development of the Quanji block from northern Tibet and the cratonic assembly of eastern Asia: American Journal of Science, v. 322, p. 705–727, doi:10.2475/05.2022.03.

Wang, R., Shen, B., Lang, X., Wen, B., Mitchell, R.N., Ma, H., Yin, Z., Peng, Y., Liu, Y., and Zhou, C., 2023a, A Great late Ediacaran ice age: National Science Review, p. nwad117, doi:10.1093/nsr/nwad117.

Wang, Z., Wang, J., Suess, E., Wang, G., Chen, C., and Xiao, S., 2017, Silicified glendonites in the Ediacaran Doushantuo Formation (South China) and their potential paleoclimatic implications: Geology, v. 45, p. 115–118, doi:10.1130/G38613.1.

Wang, R., Yin, Z., and Shen, B., 2023b, A late Ediacaran ice age: The key node in the Earth system evolution: Earth-Science Reviews, v. 247, p. 104610, doi:10.1016/j.earscirev.2023.104610.

Wang, X., Zhang, X., and Liu, W., 2021b, Biostratigraphic constraints on the age of Neoproterozoic glaciation in North China: Journal of Asian Earth Sciences, v. 219, p. 104894, doi:10.1016/j.jseaes.2021.104894.

Wilby, P.R., Carney, J.N., and Howe, M.P.A., 2011, A rich Ediacaran assemblage from eastern Avalonia: Evidence of early widespread diversity in the deep ocean: Geology, v. 39, p. 655–658, doi:10.1130/G31890.1.

Wong Hearing, T.W., Pohl, A., Williams, M., Donnadieu, Y., Harvey, T.H.P., Scotese, C.R., Sepulchre, P., Franc, A., and Vandenbroucke, T.R.A., 2021, Quantitative comparison of geological data and model simulations constrains early Cambrian geography and climate: Nature Communications, v. 12, p. 3868, doi:10.1038/s41467-021-24141-5.

Wood, R., Bowyer, F.T., Alexander, R., Yilales, M., Uahengo, C.-I., Kaputuaza, K., Ndeunyema, J., and Curtis, A., 2023, New Ediacaran biota from the oldest Nama Group, Namibia (Tsaus Mountains), and re-definition of the Nama Assemblage: Geological Magazine, v. 160, p. 1673–1686, doi:10.1017/S0016756823000638.

Wood, R., Liu, A.G., Bowyer, F., Wilby, P.R., Dunn, F.S., Kenchington, C.G., Cuthill, J.F.H., Mitchell, E.G., and Penny, A., 2019, Integrated records of environmental change and evolution challenge the Cambrian Explosion: Nature Ecology & Evolution, v. 3, p. 528–538, doi:10.1038/s41559-019-0821-6.

Woodhouse, A., Swain, A., Fagan, W.F., Fraass, A.J., and Lowery, C.M., 2023, Late Cenozoic cooling restructured global marine plankton communities: Nature, p. 1–6, doi:10.1038/s41586-023-05694-5.

Wu, C., Pang, K., Chen, Z., Wang, X., Zhou, C., Wan, B., Yuan, X., and Xiao, S., 2022, The rangeomorph fossil Charnia from the Ediacaran Shibantan biota in the Yangtze Gorges area, South China: Journal of Paleontology, p. 1–17, doi:10.1017/jpa.2022.97.

Xiao, S., Bao, H., Wang, H., Kaufman, A.J., Zhou, C., Li, G., Yuan, X., and Ling, H., 2004, The Neoproterozoic Quruqtagh Group in eastern Chinese Tianshan: evidence for a post-Marinoan glaciation: Precambrian Research, v. 130, p. 1–26, doi:10.1016/j.precamres.2003.10.013.

Xiao, S., Chen, Z., Pang, K., Zhou, C., and Yuan, X., 2021, The Shibantan Lagerstätte: insights into the Proterozoic–Phanerozoic transition: Journal of the Geological Society, v. 178, p. jgs2020-135, doi:10.1144/jgs2020-135.

Xiao, S.H., and Narbonne, G.M., 2020, Chapter 18 - The Ediacaran Period, *in* Gradstein, F.M., Ogg, J.G., Schmitz, M.D., and Ogg, G.M. eds., Geologic Time Scale 2020, Elsevier, p. 521–561, doi:10.1016/B978-0-12-824360-2.00018-8.

Xiao, Q., She, Z., Wang, G., Li, Y., Ouyang, G., Cao, K., Mason, R., and Du, Y., 2020, Terminal Ediacaran carbonate tempestites in the eastern Yangtze Gorges area, South China: Palaeogeography, Palaeoclimatology, Palaeoecology, v. 547, p. 109681, doi:10.1016/j.palaeo.2020.109681.

Yang, C., Rooney, A.D., Condon, D.J., Li, X.-H., Grazhdankin, D.V., Bowyer, F.T., Hu, C., Macdonald, F.A., and Zhu, M., 2021, The tempo of Ediacaran evolution: Science Advances, v. 7, p. eabi9643, doi:10.1126/sciadv.abi9643.

Yao, J., Xiao, S., Yin, L., Li, G., and Yuan, X., 2005, Basal Cambrian Microfossils from the Yurtus and Xishanblaq Formations (tarim, North-West China): Systematic Revision and Biostratigraphic Correlation of Micrhystridium-Like Acritarchs: Palaeontology, v. 48, p. 687–708, doi:10.1111/j.1475-4983.2005.00484.x.

Youbi, N., Ernst, R.E., Söderlund, U., Boumehdi, M.A., Lahna, A.A., Tassinari, C.C.G., Moume, W.E., and Bensalah, M.K., 2020, The Central Iapetus magmatic province: An updated review and link with the ca. 580 Ma Gaskiers glaciation, *in* Adatte, T., Bond, D.P.G., and Keller, G. eds., Mass Extinctions, Volcanism, and Impacts: New Developments, Geological Society of America, v. 544, p. 0, doi:10.1130/2020.2544(02).

Zhou, C., Li, X.-H., Xiao, S., Lan, Z., Ouyang, Q., Guan, C., and Chen, Z., 2017, A new SIMS zircon U–Pb date from the Ediacaran Doushantuo Formation: age constraint on the

Weng’an biota: Geological Magazine, v. 154, p. 1193–1201, doi:10.1017/S0016756816001175.

Zhou, C., Yuan, X., Xiao, S., Chen, Z., and Hua, H., 2019, Ediacaran integrative stratigraphy and timescale of China: Science China Earth Sciences, v. 62, p. 7–24, doi:10.1007/s11430-017-9216-2.

Zieger-Hofmann, M. et al., 2022, Correlation of Neoproterozoic diamictites in southern Namibia: Earth-Science Reviews, v. 233, p. 104159, doi:10.1016/j.earscirev.2022.104159.

**FIGURE CAPTIONS**

Table 1. Comparison of published literature compilations and correlations of candidate Ediacaran glacial deposits. Each row indicates the total number of Ediacaran glacial deposits identified by the study cited (at left), as well as their proposed association with any named glaciation. For reference, and not shown here for legibility: Tindal (2023) identified 224 potentially glaciogenic deposits with radiometric age constraints compatible with Ediacaran deposition, although poor age constraints mean many of these are likely Cryogenian in age; Youbi et al. (2020) identified 25 candidate glaciogenic deposits of Ediacaran age grouped into 12 predominantly local or regional glaciations and concluded that most were plausibly correlated with an ~580 Ma Gaskiers glaciation. See also Figure 1 and Supplementary Data 1.

| Compilation | Unique deposits | Gaskiers[a] | Fauquier[b] | Bou Azzer[c] | Hankalchough[d] | GEG[e] | Other/ Uncertain |
|---|---|---|---|---|---|---|---|
| Retallack (2022) | 31 | 4 | 5 | 9 | 12 | 0 | 0 |
| Wang et al. (2023a, b) | 39 | 0 | 0 | 0 | 0 | 39 | 0 |
| Niu et al. (2024) | 50 | 18 | 3 | 10 | 14 | 0 | 5 |

[a]Gaskiers glaciation: 581 to 579 Ma (Retallack, 2022; Niu et al., 2024).
[b]Fauquier glaciation: 572 to 570 Ma (Retallack, 2022), or 571 Ma (Niu et al., 2024).
[c]Bou Azzer: 566 to 564 Ma (Retallack, 2022), or 565 to 560 Ma (Niu et al., 2024).
[d]Hankalchough: 555 to 549 Ma (Retallack, 2022), or 563 to 551 Ma (Niu et al., 2024).
[e]Great Ediacaran Glaciation: GEG; 580 to 560 Ma or 594 to 546 Ma (Wang et al., 2023a, 2023b).

Table 2. Adaptation of Tindal's (2023) table 2.1 describing the five-star rating scheme for assessing the potential glaciogenicity of a given sedimentary deposit. Here we have added an “insufficient” zero star rating for deposits that have been interpreted as glaciogenic in the literature but do not meet the one star evidential threshold following Tindal's (2023) method. We

have also added an explicit relative weight column to illustrate the geometric growth in confidence of glaciogenicity with successive star ratings.

| Strength | Stars | Relative weight | Definition |
|---|---|---|---|
| Unequivocal | ★★★★★ | 1 | No realistic ice-free depositional environment could produce this evidence. |
| Strong | ★★★★ | 1/2 | No realistic ice-free depositional environment is likely to produce this evidence. |
| Circumstantial | ★★★ | 1/4 | This evidence could be produced by specific, but rare, ice-free depositional environments. |
| Weak | ★★ | 1/8 | Some ice-free depositional environments could produce this evidence. |
| Equivocal | ★ | 1/16 | Many ice-free depositional environments could produce this evidence. |
| Insufficient | | 0 | Many ice-free depositional environments could produce this evidence, and an ice-related origin of the observed features is not supported by the evidence. |

Table 3. Summary of the star ratings assigned to candidate Ediacaran glaciogenic deposits included in published literature compilations, presented here as the number (and percentage to nearest 1 %) of deposits of each star rating included in each compilation. Most previous compilations include a considerable number of deposits that have weak (two star or less) sedimentological or geomorphological evidence for glacial conditions. See Tindal (2023), Methods, Table 2, and Supplementary Information for methodology and ratings.

| | **Star rating** | | | | | |
|---|---|---|---|---|---|---|
| **Compilation** | Five | Four | Three | Two | One | Zero |
| Youbi et al. (2020) | 0<br>(0 %) | 10<br>(40 %) | 10<br>(40 %) | 5<br>(20 %) | 0<br>(0 %) | 0<br>(0 %) |

| | | | | | | |
|---|---|---|---|---|---|---|
| Retallack (2022) | 0 (0 %) | 7 (23 %) | 7 (23 %) | 3 (10 %) | 2 (6 %) | 12 (39 %) |
| Tindal (2023)[a] | 3 (1 %) | 62 (28 %) | 84 (38 %) | 41 (18 %) | 16 (7 %) | 18 (8 %) |
| Wang et al. (2023a, b) | 0 (0 %) | 14 (36 %) | 16 (41 %) | 5 (13 %) | 2 (5 %) | 2 (5 %) |
| Niu et al. (2024) | 1 (2 %) | 16 (32 %) | 17 (34 %) | 5 (10 %) | 3 (6 %) | 8 (16 %) |

[a]Tindal's (2023) compilation includes many deposits that are most likely Cryogenian (based on non-radiometric age constraints) in the plausible Ediacaran dataset.

Table 4. Summary of the main late Ediacaran biotic assemblages.

| Assemblage | Age range[a] | Depositional setting(s) | Morpho-groups and innovations |
|---|---|---|---|
| Avalon | <579 Ma to 565 Ma | Deep marine basin to shelf (Narbonne et al., 2014; Noble et al., 2015; Matthews et al., 2020), lacking shallow marine occurrences (Boag et al., 2024). | Complex macroscopic organisms; mostly frondose morphologies; no tubular taxa. |
| | 565 Ma to <560 Ma | Deep marine shelf to basin (Narbonne et al., 2014; Noble et al., 2015; Carbone et al., 2015; Matthews et al., 2020; Boag et al., 2024), and shallow marine, above storm wave base (Cope, 1977, 1983; Pauley, 1991; Liu, 2011; Clarke et al., 2024). | Complex macroscopic organisms; frondose morphologies; discoidal fossils both of probable frond holdfasts and individual discoidal organisms; rare simple surface trace fossils; candidate cnidarians; no or very few tubular taxa (Carbone et al., 2015); matgrounds in shallower settings. |
| White Sea | <560 Ma to >550 Ma | Marine offshore shelf to shallow shoreface (Grazhdankin, 2004; Boag et al., 2016, 2024; McMahon et al., 2020), most likely spanning all settings from near storm weather wave base to the intertidal zone (McMahon et al., 2020). | Bilaterialomorphs; first erniettomorphs; various radialomorphs; abundant non-mineralised tubular fossils (Surprenant and Droser, 2024); increasingly diverse simple trace fossils; fewer frondose fossils. |

| | | | |
|---|---|---|---|
| Nama | <550 Ma to 538.8 Ma | Marine offshore (open marine) inner shelf to reef (Boag et al., 2016, 2024; Amorim et al., 2020; Xiao et al., 2021; Wood et al., 2023; O'Connell et al., 2024), includes sites in shallow settings above storm weather wave base (Boag et al., 2016, tbl. S6; Xiao et al., 2020). | Biomineralized and soft bodied tubular fossils (Surprenant and Droser, 2024); increasingly diverse and complex trace fossils; few new frondose fossils; erniettomorphs become more prominent; candidate sponges. |

[a]The symbols ">" and "<" are used to indicate minimum and maximum constraints on age estimates for the biotic assemblages; e.g. the Avalon biotic assemblage may be at most 579 Ma and may persist in strata younger than 560 Ma.

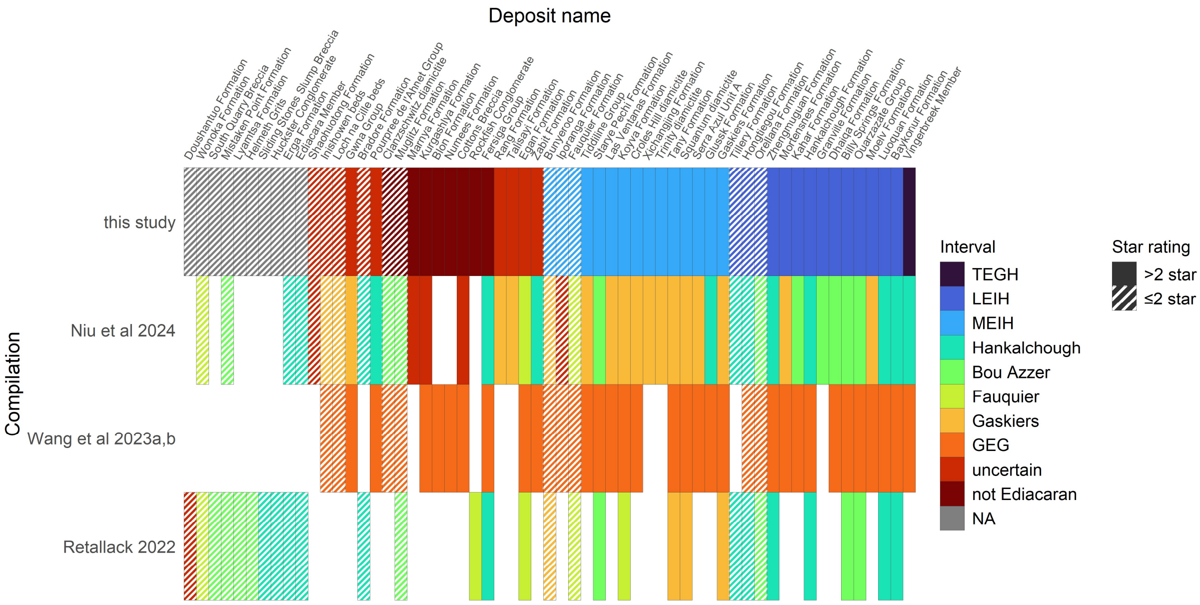


Figure 1. Comparison of the candidate Ediacaran glaciogenic deposits included in our study and in recent compilations (Retallack, 2022; Wang et al., 2023a, 2023b; Niu et al., 2024). Colors indicate the glaciation or interval the deposit was assigned to by each study. Deposits rated greater than two stars are in solid colors; deposits rated two stars or less are marked by diagonal stripes. TEGH: terminal Ediacaran greenhouse; LEIH: late Ediacaran icehouse; LEGH: late Ediacaran greenhouse; MEIH: mid-Ediacaran icehouse; GEG: Great Ediacaran Glaciation; NA:

deposits removed from consideration as candidate glaciogenic units (see Supplementary Information).

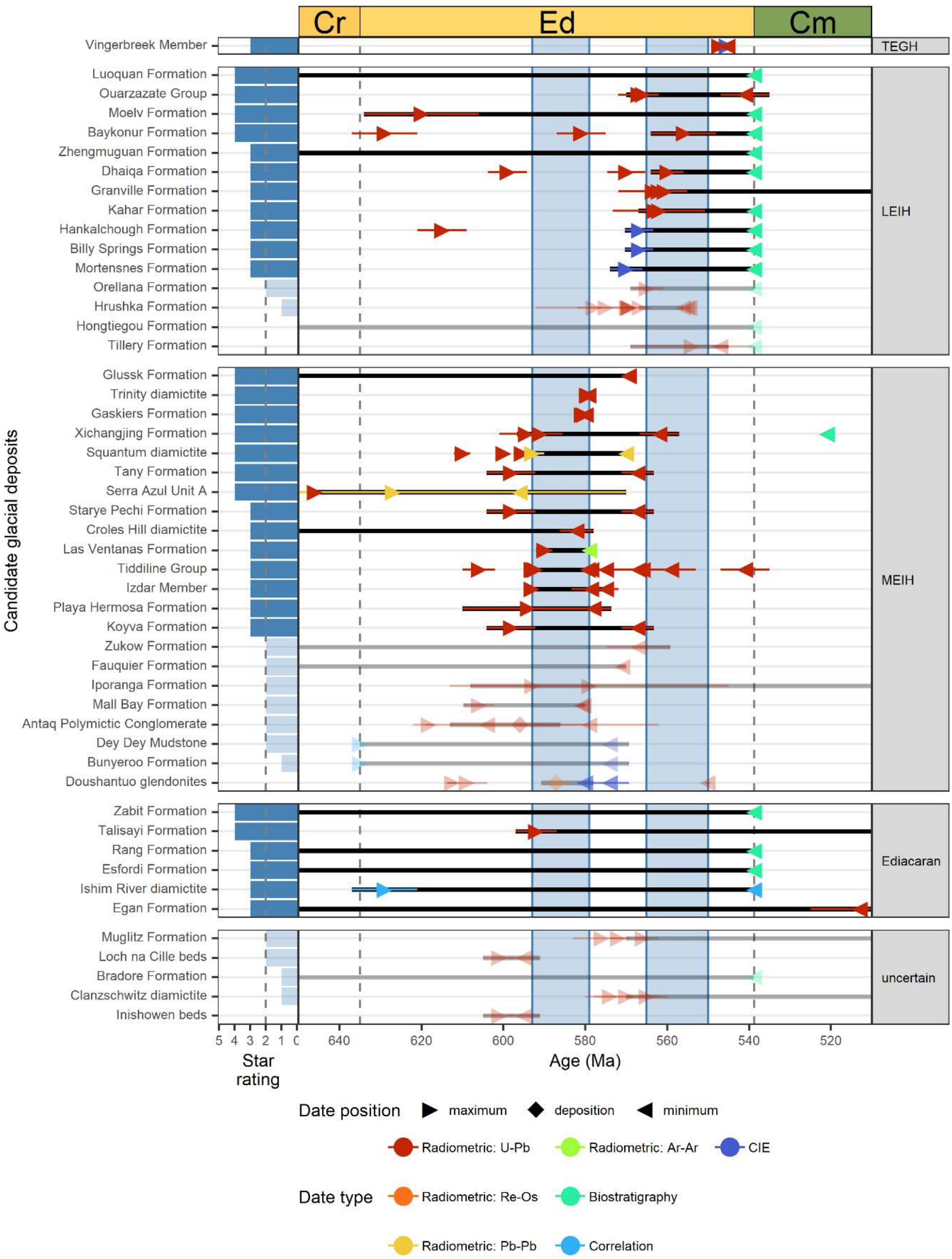
Cr
Ed
Cm
Vingerbreek Member
TEGH
Luoquan Formation
Ouarzazate Group
Moelv Formation
Baykonur Formation
Zhengmuguan Formation
Dhaiqa Formation
Granville Formation
Kahar Formation
Hankalchough Formation
Billy Springs Formation
Mortensnes Formation
Orellana Formation
Hrushka Formation
Hongtiegou Formation
Tillery Formation
LEIH
Glussk Formation
Trinity diamictite
Gaskiers Formation
Xichangjing Formation
Squantum diamictite
Tany Formation
Serra Azul Unit A
Starye Pechi Formation
Croles Hill diamictite
Las Ventanas Formation
Tiddiline Group
Izdar Member
Playa Hermosa Formation
Koyva Formation
Zukow Formation
Fauquier Formation
Iporanga Formation
Mall Bay Formation
Antaq Polymictic Conglomerate
Dey Dey Mudstone
Bunyeroo Formation
Doushantuo glendonites
MEIH
Zabit Formation
Talisayi Formation
Rang Formation
Esfordi Formation
Ishim River diamictite
Egan Formation
Ediacaran
Muglitz Formation
Loch na Cille beds
Bradore Formation
Clanzschwitz diamictite
Inishowen beds
uncertain
Candidate glacial deposits
5 4 3 2 1 0
Star rating
640 620 600 580 560 540 520
Age (Ma)
Date position
maximum
deposition
minimum
Date type
Radiometric: U-Pb
Radiometric: Ar-Ar
CIE
Radiometric: Re-Os
Biostratigraphy
Radiometric: Pb-Pb
Correlation

Figure 2. Age constraints on candidate Ediacaran glaciogenic deposits grouped by their likely depositional interval. TEGH: terminal Ediacaran greenhouse; LEIH: late Ediacaran icehouse; MEIH: mid-Ediacaran greenhouse. “Ediacaran” deposits are constrained only to the Ediacaran Period; “uncertain” deposits may be Ediacaran in age but have unreliable or disputed age constraints. Thick solid lines show the maximum permitted range for each deposit, including analytical uncertainty where relevant. Symbols show the type of constraint, i.e. whether the date provides a minimum, maximum, or depositional age for a deposit. Deposits that scoring two stars or fewer are faded. Vertical blue regions show the likely intervals of the MEIH (~593 to 579 Ma) and the LEIH (~565 to 550 Ma). Cr: Cryogenian (pars.); Ed: Ediacaran; Cm: Cambrian (pars.). See also Supplementary Data 1.

Figure 3. Representative late Ediacaran fossils of the **Avalon**, **White Sea**, and **Nama** biotic assemblages. Scale bars = 10 mm unless otherwise stated; photographed scale bar increments are cm and mm. **Nama (left to right):** *Charnia masoni*, NIGP 161628, Shibantan Member (Dengying Formation), Wuhe, South China, scale bar = 10 cm; *Helicolocellus cantori*, NIGP 176531, Shibantan Member (Dengying Formation), Wuhe, South China; *Pteridinium*, Aar Member, Farm Aar, Namibia; *Namacalathus*, Urusis Formation, Farm Swartpunt, Namibia; *Corumbella werneri*, Tamengo Formation, Corumba region, Brazil; burrows in carbonates, Shibantan Member (Dengying Formation), Wuhe, South China. **White Sea (left to right):** *Charnia masoni* (incomplete), Verkhovka Formation, Solza River, Russia; *Dickinsonia costata*, SAM P49355, Ediacara Member (Rawnsley Quartzite), Flinders Ranges, South Australia; *Kimberella quadrata*, PIN 3993/5106, Vendian Group, Zimnie Gory locality, White Sea coast, Russia; *Tribrachidium*, SAM P12898, Ediacara Member (Rawnsley Quartzite), Flinders Ranges, South Australia; *Funisia dorothea*, Ediacara Member, South Australia; *Helminthoidichnites* trace fossils, SAM P42142, Ediacara Member, Flinders Ranges (Rawnsley Quartzite), South Australia. **Avalon (left to right):** *Charnia masoni* (holotype), New Walk Museum, Leicester, Bradgate Formation, Charnwood Forest, UK; *Haootia quadriformis* (holotype), NFM F-994, Fermeuse Formation, Bonavista Peninsula, Newfoundland, Canada; *Bradgatia*, ROM 36500, Conception Group, Mistaken Point Ecological Reserve (MPER), Newfoundland, Canada; *Fractofusus andersoni*, Briscal Formation, MPER, Newfoundland, Canada; surface locomotory trace fossil, Mistaken Point Formation, MPER, Newfoundland, Canada. Abbreviations: NIGP = Nanjing Institute of Geology and Palaeontology; ROM = Royal Ontario Museum; NFM = The Rooms Provincial Museum, St. John’s, Newfoundland; SAM = South Australia Museum; PIN = Palaeontological Institute, Moscow.

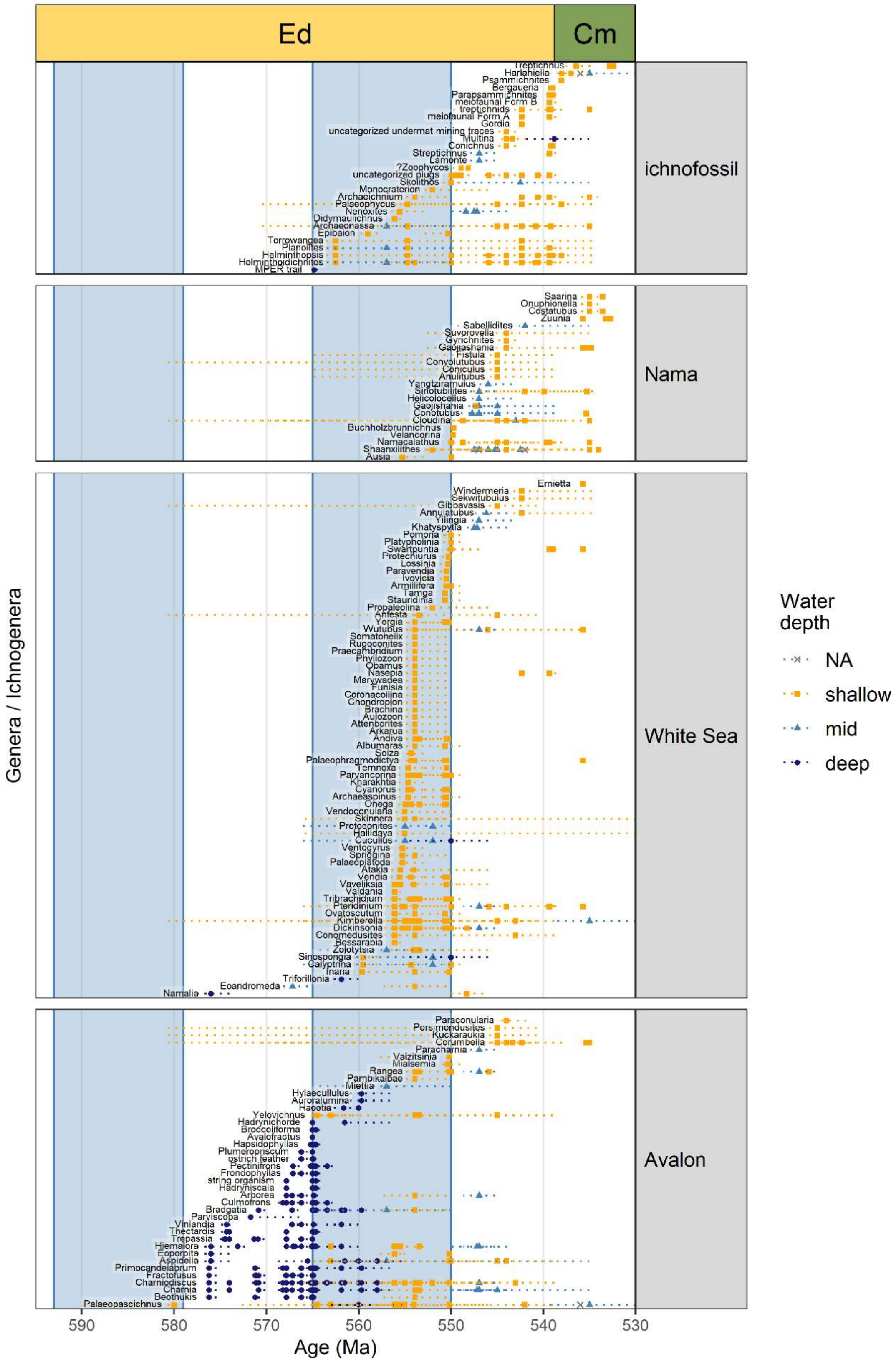
Ed
Cm
ichnofossil
Nama
White Sea
Avalon
Genera / Ichnogenera
590
580
570
560
550
540
530
Age (Ma)
Water depth
NA
shallow
mid
deep

Figure 4. Temporal distribution of Ediacaran fossil occurrences, with blue-shaded mid-Ediacaran (~593 to 579 Ma) late Ediacaran (565 to 550 Ma) icehouse climate states as inferred from well-dated glaciogenic deposits (Figure 2). Paleobiological data after: Matthews (2015); Matthews et al. (2020); Boddy et al. (2021); Bowyer et al. (2023, 2024); Surprenant and Droser (2024); and references therein. Taxa grouped into assemblages following their morphogroup assignments. Colors and shapes represent inferred water depth of each occurrence. Ed: Ediacaran; Cr: Cambrian (*pars*.). Dashed lines show the age uncertainty of each occurrence, not age range. See also Supplementary Data 2 and Figure S3.

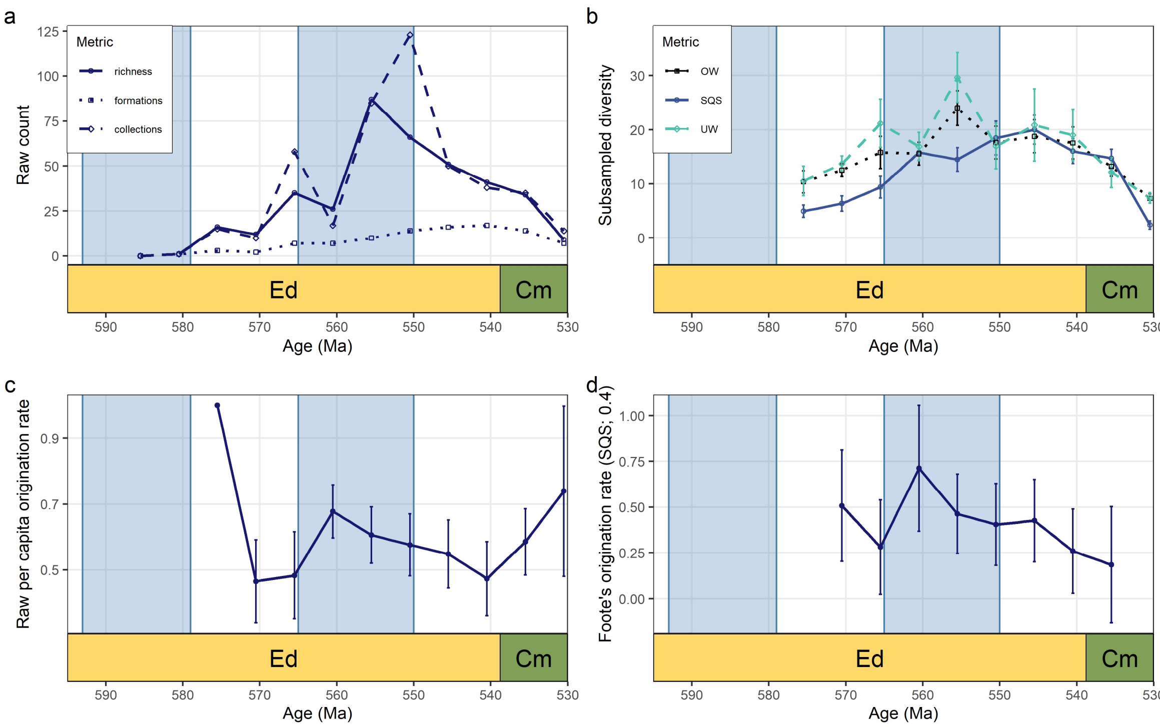


Figure 5. Paleobiodiversity metrics for the late Ediacaran biosphere. (a) Raw taxonomic richness (circles; solid lines) plotted alongside number of collections (diamonds; dashed lines) and number of formations (squares; dotted lines). (b) Subsampled taxonomic richness following

Shareholder Quorum subsampling (SQS; quota = 0.4), unweighted collection-based classical rarefaction (UW; quota = 8 collections), and occurrence-weighted subsampling (OW; quota = 14 occurrences). (c) Raw per capita origination rate for 1 Myr and 5 Myr bins. (d) SQS (quota = 0.4) subsampled Foote's origination rate for 1 Myr and 5 Myr bins. The decline in values across the Ediacaran–Cambrian boundary is an artefact of our paleobiology data compilation which focused on taxa with first occurrences in the Ediacaran Period. See also Supplementary Data 2 and Figure S4.

## SUPPLEMENTARY MATERIAL

[1]Supplemental Material. Supplementary Information: additional text and figures supporting the main manuscript; Supplementary Data 1: an Excel file of candidate Ediacaran glaciogenic deposits; Supplementary Data 2: an Excel file of Ediacaran paleontological data occurrences. Please visit https://doi.org/10.1130/XXXX to access the supplemental material, and contact editing@geosociety.org with any questions.